Chinese Journal of Natural Medicines

Predicting cerebral acetylcholine dynamics with huperzine A pharmacokinetics in blood *via* mPBPK–PD modeling

Jiaying Wang, Yangfan Zhang, Haoqian Wu, Siqi Yu, Xiaoying Cai, Youying Zhang, Jian Chen, Zixing Chen, Xiao Zheng, Haiping Hao

Citation: Jiaying Wang, Yangfan Zhang, Haoqian Wu, Siqi Yu, Xiaoying Cai, Youying Zhang, Jian Chen, Zixing Chen, Xiao Zheng, Haiping Hao, Predicting cerebral acetylcholine dynamics with huperzine A pharmacokinetics in blood *via* mPBPK–PD modeling, Chinese Journal of Natural Medicines, 2026, 24(3), 349–364. doi: 10.1016/S1875–5364(26)61109–0.

View online: https://doi.org/10.1016/S1875–5364(26)61109–0

Chinese Journal of Natural Medicines 24 (2026) 349-364

Contents lists available at ScienceDirect

Chinese Journal of Natural Medicines

journal homepage: www.cjnmcpu.com/

Original article

Predicting cerebral acetylcholine dynamics with huperzine A pharmacokinetics in blood *via* mPBPK-PD modeling

Jiaying Wang[a,b,Δ], Yangfan Zhang[a,b,Δ], Haoqian Wu[a,b], Siqi Yu[a,b], Xiaoying Cai[a,b], Youying Zhang[a,b], Jian Chen[a,b], Zixing Chen[a,b], Xiao Zheng[a,b,*], Haiping Hao[a,b,*]

[a] *State Key Laboratory of Natural Medicines*, *China Pharmaceutical University*, *Nanjing 211198*, *China*
[b] *Laboratory of Metabolic Regulation and Drug Target Discovery*, *School of Pharmacy*, *China Pharmaceutical University*, *Nanjing 210009*, *China*

ARTICLE INFO

Article history:
Received 23 February 2025
Revised 13 May 2025
Accepted 15 May 2025
Available online 20 March 2026

Keywords:
Huperzine A
Acetylcholinesterase
Neuroprotection
Acetylcholine
Ischemic stroke
mPBPK-PD
MCAO model

ABSTRACT

Huperzine A (HupA) is a highly selective, reversible acetylcholinesterase (AChE) inhibitor that exhibits neuroprotective effects and is clinically used to manage benign memory decline. However, the specific relationship between the pharmacokinetic (PK) profile of HupA and cerebral acetylcholine (ACh) dynamics remains poorly characterized. Here, we characterize the PK-pharmacodynamic (PD) properties of HupA in rats under both physiological and pathological conditions. Following a single intramuscular injection, HupA exhibits a short half-life but rapid brain penetration, while multiple dosing significantly enhances its brain exposure. In a middle cerebral artery occlusion (MCAO) rat model, HupA demonstrates increased brain distribution. Furthermore, HupA elevates ACh concentrations across multiple brain regions, concurrently modulating several monoamine neurotransmitters. Using a minimal physiologically based pharmacokinetic-pharmacodynamic (mPBPK-PD) modeling approach, cerebral ACh dynamics were accurately predicted based on the pharmacokinetics of HupA in systemic circulation. The developed mPBPK-PD model exhibits robust predictive performance and holds potential for guiding the optimization of clinical dosing regimens and improving the therapeutic efficacy of HupA.

1. Introduction

Huperzine A (HupA) is a sesquiterpenoid alkaloid derived from the Chinese herb *Huperzia serratum* Thunb. [1, 2]. As a potent and selective inhibitor of acetylcholinesterase (AChE), HupA acts reversibly and has demonstrated neuroprotective properties [3]. It is clinically used to treat memory disorders in the elderly and to address cognitive dysfunction associated with cholinergic deficits in the brain [4, 5]. Moreover, extensive studies have shown that HupA confers neuroprotection against ischemia-induced injury, both *in vitro* and *in vivo*, primarily through its cholinergic anti-inflammatory effects [6, 7]. HupA has also been reported to significantly improve cognitive function in patients with Alzheimer's disease (AD) and vascular dementia (VaD) [8], and it exhibits neuroprotective effects in epilepsy [9]. Furthermore, long-term administration of HupA has been found to alleviate post-stroke depression (PSD) and cognitive impairments in rat models, likely mediated by its regulatory effects on neurotransmitters and neurotrophic factors in the brain [10]. Accumulating evidence indicates that HupA enhances neuronal survival and promotes axonal regeneration [11–13]. These findings underscore the broad therapeutic potential of HupA in the treatment of neurological disorders.

As a prototypical AChE inhibitor, the pharmacological activity of HupA is closely tied to modulation of acetylcholine (ACh) levels [14]. However, HupA exhibits poor water solubility and limited oral bioavailability, although these challenges can be mitigated through optimized formulations and alternative routes of administration [12, 15, 16]. Clinically, HupA is commonly administered *via* injection (huperzine A injection, HAI) for benign memory complaints and myasthenia gravis, and its application is increasingly expanding to include AD and other forms of cognitive impairment [17, 18]. Notably, HAI has been shown to improve motor function and cognitive performance in mouse models of Parkinson's disease [19]. Despite these advances, the pharmacokinetics (PK) of HAI and its relationship with pharmacodynamic (PD) outcomes remain insufficiently characterized. In particular, the association between systemic exposure to HupA and regional dynamics of ACh in the brain remains poorly understood. This knowledge gap is particularly critical for central nervous system (CNS)-targeted drugs, as maintaining optimal ACh concentrations in specific brain regions is essential for maximizing therapeutic efficacy [20].

The minimal physiologically based PK-PD (mPBPK-PD) model is a simplified physiology-based PK framework that integrates microphysiological principles with PK (PBPK) and PD modeling. The mPBPK approach was first introduced by Cao and Jusko in 2013 [21]. Compared to conventional systemic PBPK models, the mPBPK model improves computational efficiency and simulation speed by reducing the complexity of multi-organ or tissue com-

* Corresponding author.
E-mail addresses: xzheng@cpu.edu.cn (X. Zheng); haipinghao@cpu.edu.cn (H. Hao)
Δ These authors contributed equally to this work.

https://doi.org/10.1016/S1875-5364(26)61109-0

partments. While preserving the core physiological relevance of systemic PBPK models, it focuses specifically on drug actions within target tissues using physiologically meaningful parameters. To date, the mPBPK model has been applied to the evaluation of various biotherapeutics [22, 23]. Integrating PBPK and PD components enables the prediction of drug responses under different dosing regimens and accounts for inter-individual variability.

In this study, we investigated the PK profile of HAI in rat plasma under both normal physiological conditions and the pathological state induced by middle cerebral artery occlusion (MCAO)-associated cognitive impairment. Using microdialysis, we examined the distribution of HupA across multiple brain regions and monitored changes in ACh levels in these areas under both physiological and pathological conditions [24, 25]. By integrating PK data from plasma, brain tissue, cerebrospinal fluid (CSF), and extracellular fluid (ECF), we developed an mPBPK model for HupA. This model was employed to predict and simulate temporal drug concentration profiles in plasma and discrete brain regions. Furthermore, by incorporating ACh dynamics as a PD endpoint, we established a comprehensive PK-PD model, enabling prediction of cerebral ACh responses under various HAI dosing protocols and providing a rational basis for individualized dose optimization.

2. Materials and methods

2.1. Chemicals and reagents

HupA standard (purity > 97%) and HupA injections (0.3 $mg{\cdot}mL^{-1}$) were provided by WEPON Pharmaceutical Company (Zhejiang, China). Heparin sodium salt, formic acid, and ammonium formate were purchased from Aladdin Biochemical Science and Technology (Shanghai, China) and RHAWN (Shanghai, China). Standards of ACh, 5-hydroxytryptamine (5-HT), 5-hydroxyindoleacetic acid (5-HIAA), dopamine (DA), norepinephrine (NE), adrenaline (Adr), gamma-aminobutyric acid (γ-GABA), glutamate (Glu), and aspartic acid (Aspa) were obtained from Sigma-Aldrich (USA). Acetonitrile and methanol (LC-MS grade) were acquired from Merck (Germany), and all other reagents were of analytical grade or the highest commercially available grade. HupA standard stock solutions were prepared by dissolving HupA in methanol to yield a final concentration of 1.0 $mg{\cdot}mL^{-1}$.

2.2. Animals

Specific pathogen-free (SPF) male Sprague-Dawley rats (200 ± 20 g) were obtained from Beijing Vital River Laboratory Animal Technology Co. (Certificate No. SCXK 2019-0001) and housed individually in standard cages under controlled conditions: relative humidity (RH) 50% ± 5%, temperature 22 ± 1 °C, and a 12-h light/dark cycle (lights on at 07:00, off at 19:00), with *ad libitum* access to food and water. All animal procedures were approved by the Animal Ethics Committee of China Pharmaceutical University. Measures were taken to minimize animal discomfort throughout the experimental period.

2.3. Preparation of MCAO model rats

Male Sprague-Dawley rats (260–270 g) underwent transient MCAO using the intraluminal filament method [26, 27]. Briefly, animals were anesthetized with isoflurane and placed on a heating pad to maintain rectal temperature at 37.0 ± 0.5 °C. A midline neck incision was made to expose the left common carotid artery (CCA), internal carotid artery (ICA), and external carotid artery (ECA). A nylon filament (18.5 ± 0.5 mm in length) was inserted *via* the CCA into the ICA to occlude the origin of the middle cerebral artery. After 2 h of occlusion, the filament was gently withdrawn to initiate reperfusion. Sham-operated rats underwent identical surgical procedures without filament insertion. Neurological deficits in MCAO rats were assessed using the Longa neurological scoring system [26].

2.4. Measurement of infarct size and brain water content

Twenty-four hours after ischemia-reperfusion (n = 10), rats were anesthetized and perfused with saline *via* the left ventricle. Brains were rapidly excised, weighed, and frozen at −20 °C for 30 min. Five 2 mm-thick coronal brain sections were incubated in 1% 2,3,5-triphenyltetrazolium chloride (TTC) at 37 °C for 20 min in the dark, then fixed in 4% paraformaldehyde at 4 °C for at least 6 h. Infarct areas were quantified using ImageJ software, with ischemic area expressed as a percentage of total hemispheric area (n = 5).

$$\text{Ratio of cerebral infarction}\ (\%) = \frac{\textit{Ischemic infarct area}}{\textit{Ischemic hemisphere area}} \times 100 \quad (1)$$

For brain water content analysis, brain tissues (n = 10) were rinsed with ice-cold PBS (4 °C), blotted dry, and immediately weighed (wet weight). Tissues were dried at 70 °C for 24 h to constant weight and reweighed (dry weight). The water content was calculated using the following formula:

$$\text{Water content of brain Tssiue}\ (\%) = \frac{\textit{Wet weight} - \textit{Dry weight}}{\textit{Wet weight}} \times 100 \quad (2)$$

2.5. Laser speckle contrast imaging to monitor brain blood flow

Ten rats (n = 10) were anesthetized and secured onto a stereotaxic frame. Head hair, including over the surgical site, was shaved, and the skull was exposed. The surface fascia was carefully cleaned using cotton swabs. The probe of a dual-wavelength laser Doppler blood flow instrument (moorFLPI-2, MOOR, UK) was positioned perpendicularly above the exposed skull and fixed in place. Cortical blood flow (CBF) was monitored and recorded in real time before ischemia, during ischemia, and after reperfusion. Images were acquired using the MoorLDI 6.0 image acquisition system.

2.6. PK study

In the single-dose PK study, rats (n = 6 per group) were acclimated for five days, fasted for 24 h, and administered HupA intramuscularly at doses of 0.1, 0.3, or 0.5 $mg{\cdot}kg^{-1}$. Blood samples (500 μL) were collected from the retro-orbital sinus at 0 h (predose) and at 0.05, 0.083, 0.17, 0.25, 0.33, 0.5, 0.75, 1, 1.5, 2, 4, 6, and 8 h post-dose. For the multiple-dose PK study, a second group (n = 6) received daily intramuscular doses of 0.3 $mg{\cdot}kg^{-1}$ HupA for five consecutive days. Blood samples were collected on days 1 and 5 at the same time points, as well as at 15 min, 1 h, and 24 h post-dose from day 2 to day 4.

A third group (n = 6 per group) was used for CSF and arterial blood sampling. Rats were administered 0.3 $mg{\cdot}kg^{-1}$ HupA intramuscularly, and CSF was collected *via* cisterna magna puncture at 3, 15, and 30 min, and 1, 4, and 6 h post-dose. Both blood and CSF samples were centrifuged at 8000 $r{\cdot}min^{-1}$ for 5 min. A fourth group (n = 6 per group) was designated for tissue distribution studies following single and multiple 0.3 $mg{\cdot}kg^{-1}$ doses. Animals were euthanized at 5 and 15 min, and 4 and 6 h post-dose. Tissues, including abdominal muscles, stomach, jejunum, testes, pancreas, spleen, heart, liver, kidneys, and discrete brain regions, were harvested. In the multiple-dose group, 0.3 $mg{\cdot}kg^{-1}$ HupA

was administered daily for five days, with tissue samples collected at corresponding time points on day 5. All samples, including blood, CSF, and tissues, were stored at −80 °C until analysis.

2.7. Cerebral microdialysis

Eight male Sprague-Dawley rats (200 ± 20 g) were fasted for 24 h and administered 0.3 mg·kg^{-1} HupA intramuscularly. Surgical instruments were sterilized with alcohol, and a 1 mm diameter craniotomy was drilled at the predetermined site. A guide cannula was implanted into the brain, secured with dental cement, and the wound was sutured and disinfected. Following a recovery period of 4–5 days, rats were connected to a microdialysis system (Eicom). A microdialysis probe was inserted into the CA1 region of the hippocampus (Hc), and artificial CSF was perfused at 0.2 μL·min^{-1} for 1.5 h, followed by collection of baseline dialysate samples every 20 min for 1 h.

Subsequently, 0.3 mg·kg^{-1} HupA was administered intramuscularly at 9:00 AM. Dialysate samples were collected at 10-min intervals for the first hour, every 20 min for the next hour, every 30 min between 2 and 4 h, hourly from 4 to 8 h, and finally every 2 h from 8 to 10 h. Samples were collected under dark, low-temperature conditions and stored at −80 °C. For analysis, 15 μL of dialysate was mixed with 5 μL of internal standard solution [200 ng·mL^{-1} 1-methylthymine (1-MT), 100 ng·mL^{-1} scopolamine hydrobromide (SH)], vortexed, and 5 μL was injected into the analytical system. HupA concentrations in the hippocampal CA1 region were determined using a pre-established quantitative calibration curve.

2.8. Quantitative analysis of HupA biological samples using liquid chromatography-tandem mass spectrometry (LC-MS/MS)

2.8.1. Sample preparation

Plasma (50 μL) and homogenized tissue samples (5 mg in 50 μL ultrapure water) were subjected to protein precipitation. Methanol (400 μL) containing scopolamine hydrobromide (100 ng·mL^{-1}) as internal standard was added to each sample. After vortexing for 15 min, mixtures were centrifuged at 18,000 r·min^{-1} for 10 min. The supernatant (350 μL) was concentrated under vacuum for 4 h, reconstituted in 100 μL pure methanol, vortexed for 15 min, and centrifuged twice at 18 000 r·min^{-1} for 10 min prior to injection.

2.8.2. LC-MS/MS conditions

Quantification was performed using an LC-20AD liquid chromatography system (Shimadzu, Japan) coupled to an API 4000 + tandem mass spectrometer (AB Sciex, USA). The mobile phase consisted of 0.05% formic acid in 5 mmol·L^{-1} ammonium formate (phase A) and acetonitrile (phase B). Chromatographic separation was achieved on a Phenomenex Luna C_{18} column (150 mm × 2.00 mm, 5 μm) maintained at 40 °C, with a flow rate of 0.3 mL·min^{-1} and an injection volume of 10 μL. Gradient elution was programmed as follows: 0–1.5 min, 10% B; 1.5–2 min, 10%→90% B; 2–5.5 min, 90% B; 5.5–6 min, 90%→10% B; 6–8 min, 10% B.

The mass spectrometer operated in positive electrospray ionization (ESI) mode with multiple reaction monitoring (MRM). Key parameters included: spray voltage 5500 V, curtain gas 20 psi, collision gas 8 psi, ion source gases 1 and 2 set at 55 and 50 psi, respectively, and a source temperature of 550 °C. Mass spectrometric parameters for HupA are listed in Table1.

2.8.3. Method validation

2.8.3.1 Linearity and lower limit of quantification (LLOQ)

Plasma calibration standards were prepared by adding 5 μL of HupA standard solutions to 45 μL of blank rat plasma, yielding concentrations of 0.5, 1, 5, 10, 50, 100, and 500 ng·mL^{-1}. Additionally, double blank plasma (DB) and plasma containing only the internal standard SH (CB) were prepared. Linearity was evaluated using weighted linear regression ($1/x^2$), plotting the peak area ratio of HupA to IS against nominal concentration. The intra-day precision (relative standard deviation (RSD), %) at the LLOQ and accuracy (RE, %) were required to remain within ±20%.

2.8.3.2 Accuracy and precision

Forty-five microliters of blank rat plasma were spiked with 5 μL of HupA standards to prepare quality control (QC) samples at 1, 50, and 375 ng·mL^{-1} and an LLOQ sample at 0.5 ng·mL^{-1} (n = 5). Samples were processed and analyzed, and concentrations were back-calculated using the calibration curve. Each concentration was tested in quintuplicate daily over three days to assess intra- (n = 5) and inter-batch (n = 15) variability. Acceptance criteria were RSD ≤ 15% and RE within ±15% for QC samples, and RSD ≤ 20% and RE within ±20% for the LLOQ.

2.8.3.3 Extraction recovery and matrix effect

For extraction recovery, 45 μL of blank plasma was spiked with 5 μL of HupA at 1, 50, and 375 ng·mL^{-1}, followed by methanol precipitation and analysis (n = 5). A parallel set was prepared by spiking HupA into the supernatant after protein precipitation. Recovery was calculated based on the ratio of peak areas. For assessment of matrix effect, analyte responses in plasma extracts were compared to those in pure solvent, and the matrix factor was derived from the peak area ratio.

2.8.3.4 Stability

Stability of HupA in spiked plasma (1, 50, 375 ng·mL^{-1}, n = 5) was evaluated under various conditions: room temperature for 4 h, in the autosampler at 4 °C for 24 h, after three freeze-thaw cycles, and during storage at −20 °C for two weeks.

2.9. Quantitative analysis of neurotransmitters in the rat brain

Sample preparation and MS conditions were consistent with those described above. Quantitative analysis was conducted us-

Table 1 Mass spectrometry analysis parameters (HupA, neurotransmitters, and SH).

Compound	m/z[a]		CE[b] (eV)	DP[b] (eV)
	Q1[a]	Q3[a]		
HupA	243.3	210.2	38	100
SH	304.2	138.2	27	65
ACh	146.2	87.0	60	17
rGABA	103.9	87.0	42	14
5-HT	177.0	160.0	40	5
5-HIAA	192.0	146.0	60	20
Aspa	134.3	74.0	50	19
Adr	184.6	167.2	50	15
Glu	148.2	84.0	130	17
DA-1	154.2	90.9	40	15
DA-2	154.5	138.1	50	15
NE	170.0	152.0	40	15
1-MT	219.2	160.0	55	25
SCP	304.2	138.2	65	27

[a]m/z, mass-to-charge ratio; Q1, Quadrupole 1, acts as a mass filter to select precursor ions based on their m/z values; Q3, Quadrupole 3, analyzes product ions by selecting fragment ions for further investigation. [b]DP, Declustering potential, reduces ion-neutral interactions, improving ion separation and sensitivity; and CE, Collision energy, induces ion fragmentation in the collision cell, providing structural information on the analyte.

ing an LC-20AD liquid chromatography system (Shimadzu, Japan) coupled with an API 4000+ tandem mass spectrometer (AB Sciex, USA). The mobile phase consisted of 0.05% formic acid in 5 mmol·L^{-1} ammonium formate (phase A) and acetonitrile (phase B). Separation was achieved on a Waters Atlantis T3 column (3 μm, 2.1 mm × 100 mm, USA) at 40 °C, with a flow rate of 0.3 mL·min^{-1} and an injection volume of 10 μL. Gradient elution was set as follows: 0–3 min, 5% B; 3–5 min, 5%→65% B; 5–8 min, 65%→95% B; 8–12 min, 95% B. Mass spectrometry was performed in positive ESI mode with MRM. Instrumental settings included: spray voltage at 5500 V, curtain gas at 20 psi, collision gas at 8 psi, ion source gases 1 and 2 at 55 and 50 psi, respectively, and a source temperature of 550 °C. Mass spectrometric parameters for HupA and target neurotransmitters are listed in Table1. The total scan time (including pauses) was 2.3001 s. Summary of the acquisition period: duration of 16.999 min, delay time of 0 s, totaling 635 cycles with a cycle time of 2.3001 s.

2.10. mPBPK modeling and PK/PD simulation

The primary software tools used for model development included: (1) Engauge Digitizer 12.1 for data digitization; (2) Monolix Suite 2019R2, a platform employing the stochastic approximation expectation maximization (SAEM) algorithm and Markov chain Monte Carlo (MCMC) methods for non-linear mixed-effects (NLME) modeling [28]. Monolix Suite was utilized to establish and optimize population PK (pop PK), PK-PD, and quantitative systems pharmacology (QSP) models [29, 30]; (3) Additional software included Berkeley Madonna 10.2.8, R 4.1.2, and RStudio 1.3.1037. A literature search was conducted in PubMed and Web of Science using the keywords "huperzine A and pharmacology and rat" and "huperzine A and pharmacology and human". Retrieved articles were manually screened according to the following criteria: (1) intramuscular administration of HupA; (2) exclusion of formulations affecting PK, such as nano-preparations; and (3) absence of co-administered drugs to prevent PK interactions. Data from selected studies were extracted using Engauge Digitizer 12.1 and compiled into a CSV file containing dosage, administration frequency, sampling time, drug concentration, and detection method. These data were subsequently used in Monolix Suite 2019R2 and other software for PK model development.

Accurate quantification of regional brain concentrations is essential for refining PBPK models of CNS drugs, particularly those exhibiting heterogeneous brain distribution. We conducted PK analysis and developed a rat CNS PBPK model incorporating the Hc, CSF, and whole-brain ECF to predict HupA disposition [31]. A diffusion-rate-limited approach was employed to describe HupA distribution from plasma to CSF and Hc, dividing the brain into vascular, hippocampal, other brain parenchyma, and CSF compartments. HupA was administered intramuscularly, absorbed into the central compartment (Vc), and eliminated (ke). The drug entered the cerebral vasculature (Q_b), crossed the blood-brain barrier (BBB) with a permeability-surface area product (PS_{BBB}), entered the Hc and the rest of brain mass (RBM), and subsequently diffused into the CSF. Since HupA is a substrate of BBB efflux transporters, V_{max} and K_m were incorporated. Distinct permeation parameters were applied for the blood-CSF barrier. Efflux clearance (Clout) provided adequate model fit; therefore, Michaelis-Menten kinetics were omitted for simplification.

Based on the constructed PK model, ACh concentrations in the Hc and ECF were integrated as PD endpoints. In the PD model, a kin/kout model (indirect response model) was applied to describe ACh dynamics in the Hc and interstitial fluid, assuming steady-state levels under baseline conditions. Upon drug administration, AChE inhibition reduces ACh elimination, resulting in elevated ACh concentrations. Concurrently, intracellular accumulation promotes ACh exocytosis into the interstitial fluid. The final model structure, illustrated in Fig. 1, integrates both PBPK and PD components.

The ordinary differential equations (ODEs) of the model are as follows:

(1) Concentration of HupA in the central compartment:

$$Vc \times \frac{dCc_{HupA}}{dt} = ka \times Aa - k \times Ac - Qb \times (Cc - Cv) \quad (3)$$

(2) Concentration of HupA in cerebral vessels:

$$Vv \times \frac{dCv_{Brain}}{dt} = Qb \times (Cc - Cv) - PS_{Hc} \times (Cv \times fu_{plasma} - Cu_{Hc}) - PS_{Hc} \times (Cv \times fu_{plasma} - Cu_{oth}) + \frac{Cl_{max}Cu_{Hc}}{Cl_{50} + Cu_{Hc}} + \frac{Cl_{max}Cu_{oth}}{Cl_{50} + Cu_{oth}} - PS \times (Cv \times fu_{plasma} - C_{CSF}) + Cl_{CSF} \times C_{CSF} \quad (4)$$

(3) Concentration of drug in CSF:

$$V_{CSF} \times \frac{dC_{CSF}}{dt} = PS \times (Cv \times fu_{plasma} - C_{CSF}) - Cl_{CSF} \times C_{CSF} + Qs_{in}k_{hc} \times Cu_{Hc} + Qs_{in}k_{oth} \times Cu_{oth} \quad (5)$$

(4) Concentration of drug in Hc:

$$V_{Hc} \times \frac{dCc_{hc}}{dt} = PS_{Hc} \times (Cv \times fu_{plasma} - Cu_{Hc}) - \frac{Cl_{max}Cu_{Hc}}{Cl_{50} + Cu_{Hc}} - Qs_{in}k_{hc} \times Cu_{Hc} \quad (6)$$

(5) Free drug concentrations in other brain tissue:

$$V_{oth} \times \frac{dC_{oth}}{dt} = PS_{Hc} \times (Cv \times fu_{plasma} - Cu_{oth}) - \frac{Cl_{max}Cu_{oth}}{Cl_{50} + Cu_{oth}} - Qs_{in}k_{oth} \times Cu_{oth} \quad (7)$$

The parameters are detailed in Table 2, and the PK-PD model solution involves the parameters presented in Table 3.

2.11. Statistical analysis

PK parameters, including area under the curve and half-life ($t_{1/2}$), were estimated using non-compartmental analysis (NCA)

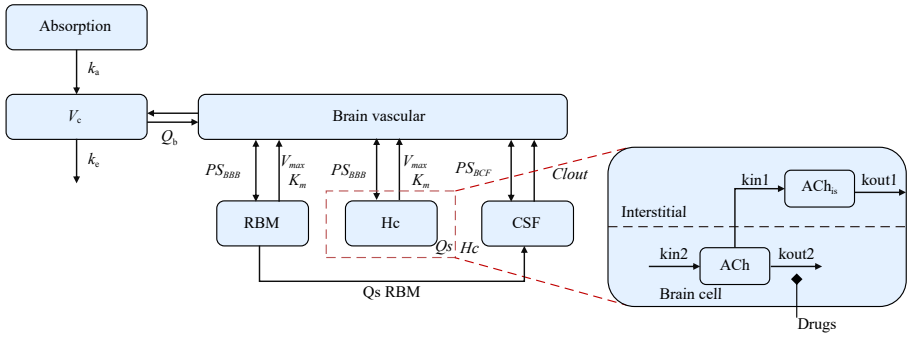

Fig. 1 Schematic of the mPBPK-PD model for HupA in rats. ACh, concentration of ACh in the hippocampal; AChis, concentration of ACh in the hippocampal interstitial fluid text; kin1, Production rate of acetylcholine in the interstitial fluid; kout1, Elimination rate of acetylcholine in the interstitial fluid; Other parameters are detailed in the main.

Table 2 List of variables and parameters of the HupA pharmacokinetic model.

Parameter name/variable name	Concepts	Unit
A_a	The amount of the drug in the absorption chamber	ng
C_c	Central chamber drug concentration	ng·mL^{-1}
C_v	Drug concentration in cerebrovascular	ng·mL^{-1}
A_c	Amount of central chamber drugs	ng
C_{Hc}	Concentration of drugs in the hippocampus	ng·mL^{-1}
Cu_{Hc}	Free drug concentration in the hippocampus	ng·mL^{-1}
C_{CSF}	Concentration of drugs in cerebrospinal fluid	ng·mL^{-1}
C_{oth}	Drug concentrations in other brain parenchymal compartments	ng·mL^{-1}
Av_{brain}	The amount of drugs in the cerebrovascular	ng
A_{Hc}	Amount of drugs in the hippocampus	ng
A_{oth}	Amount of other brain parenchymal compartment drugs	ng
A_{CSF}	The amount of drugs in the cerebrospinal fluid	ng
fu_{plasma}	Free fraction of staphylococcinolone acetonide in plasma	-
V_{brain}	Volume of rat brain	mL
Q_b	Blood flow in the rat brain	mL·h^{-1}
V_v	Volume of cerebral vessels	mL
V_{Hc}	Volume of the hippocampus in rats	mL
V_{oth}	Volume of other brain parenchymal compartments in rats	mL
V_{CSF}	Cerebrospinal fluid volume in rats	mL
$Qs_{in}k_{hc}$	Fluid from the hippocampal flow to the cerebrospinal fluid	mL·h^{-1}
$Qs_{in}k_{oth}$	Flow from other parenchymal compartments to cerebrospinal fluid	mL·h^{-1}
k_a	Absorption rate of the drug	h^{-1}
k (k_e)	Elimination rate of the drug	h^{-1}
V (V_c)	Volume of the drug central chamber	mL
PS_{BCSF}	Permeation rate of the blood-cerebrospinal fluid barrier of drugs	mL·h^{-1}
fu_{Hc}	Free fraction of drugs in the hippocampus	-
Cl_{max} (V_{max})	Maximum rate of efflux transporters on BBB	ng·h^{-1}
Cl_{50} (K_m)	Drug concentration at half the maximum transport rate of efflux transporters on the BBB	ng·mL^{-1}
Cl_{CSF}	Efflux rate of efflux transporters on the BBB fluid barrier	mL·h^{-1}
PS_{Hc} (PS_{BBB})	The rate of penetration of the blood-brain barrier of drugs	mL·h^{-1}

in Phoenix WinNonlin 8.3. Compartmental PK models were also developed and optimized as appropriate. Statistical analyses and data processing were conducted using GraphPad Prism® 9.5.0 (San Diego, CA, USA) and ImageJ. Data are presented as mean ± standard error of the mean (SEM). Repeated measures analysis was applied where applicable. Group comparisons were performed using an unpaired *t*-test for two groups and one-way ANOVA for more than two groups. A *P*-value < 0.05 was considered statistically significant. Significance levels are denoted as follows: $^{*}P < 0.05$, $^{**}P < 0.01$, $^{***}P < 0.001$, $^{****}P < 0.0001$.

Table 3 Solution of pharmacokinetic and pharmacodynamic model parameters for HupA.

Parameters	Value	CV (%)	Source
k_a	0.656	17.8	Estimated
k (k_e)	19.6	12.1	Estimated
V (V_c)	12.5	14.6	Estimated
PS_{BCSF}	0.365	28.3	Estimated
fu_{Hc}	0.150	-	Fixed
Cl_{max} (V_{max})	56.1	24.6	Estimated
Cl_{50} (K_m)	16.1	27.6	Estimated
Cl_{CSF}	0.724	17.1	Estimated
PS_{Hc} (PS_{BBB})	0.200	13.6	Estimated
kout1	6.56	66.7	Estimated
k1	0.0241	24.9	Estimated
kout2	10.3	35.5	Estimated
I_{max}	0.450	29.7	Fixed
IC_{50}	15.3	19.6	Estimated

3. Results

3.1. Plasma PK of HupA in rats under single and multiple dosing regimens

To accurately measure HupA dynamics in biological samples, an LC-MS/MS quantitative method was developed and validated. The method demonstrated adequate sensitivity and specificity, with retention times of 4.46 min for HupA and 4.45 min for IS (Fig. 2A). HupA exhibited a linear response across the concentration range of 0.5–500 ng·mL^{-1} in plasma ($y = 0.003\ 22x + 0.000\ 030\ 3$, $r = 0.9979$), with a LLOQ of 0.5 ng·mL^{-1} (Fig. 2B). Precision, accuracy, extraction recovery, matrix effects, and stability under various conditions are summarized in Supplemental Tables 1–3. Interday variability for HupA at concentrations of 0.5, 1, 50, and 375 ng·mL^{-1} was below 15%. Extraction recoveries at QC levels (1, 50, 375 ng·mL^{-1}) exceeded 90%, and matrix effects ranged from 96.51% to 101.70%. Stability assessments confirmed that HupA remained stable in plasma under various conditions, including storage at room temperature for 4 and 24 h, 48 h in an autosampler, three freeze–thaw cycles, and storage at −20 °C for two weeks, with RSD consistently below 15%. These results confirm that the LC-MS/MS method met all bioanalytical validation criteria for plasma sample analysis.

As shown in Fig. 2C, following a single intramuscular injection of HAI at doses of 0.1, 0.3, and 0.5 mg·kg^{-1} in rats, plasma HupA rapidly reached peak concentration and was quickly eliminated, with a half-life of approximately 1.10 h. Non-compartmental PK parameters are presented in Table 4. Based on the residual weighted sum of squares, Akaike information criterion (AIC), and Bayesian information criterion (BIC), a compartmental model was selected using Phoenix WinNonlin (Table 5). Linear regression analysis of the three dose levels against their corresponding area under the concentration-time curve (AUC) values (Fig. 2D) indicated dose-proportional exposure, consistent with linear PK for HupA.

According to data from the Shanghai Institute of Materia Medica [32], the IC_{50} value of HupA for inhibiting AChE is 46.2 nmol·L^{-1}, corresponding to a calculated serum 90% effective max-

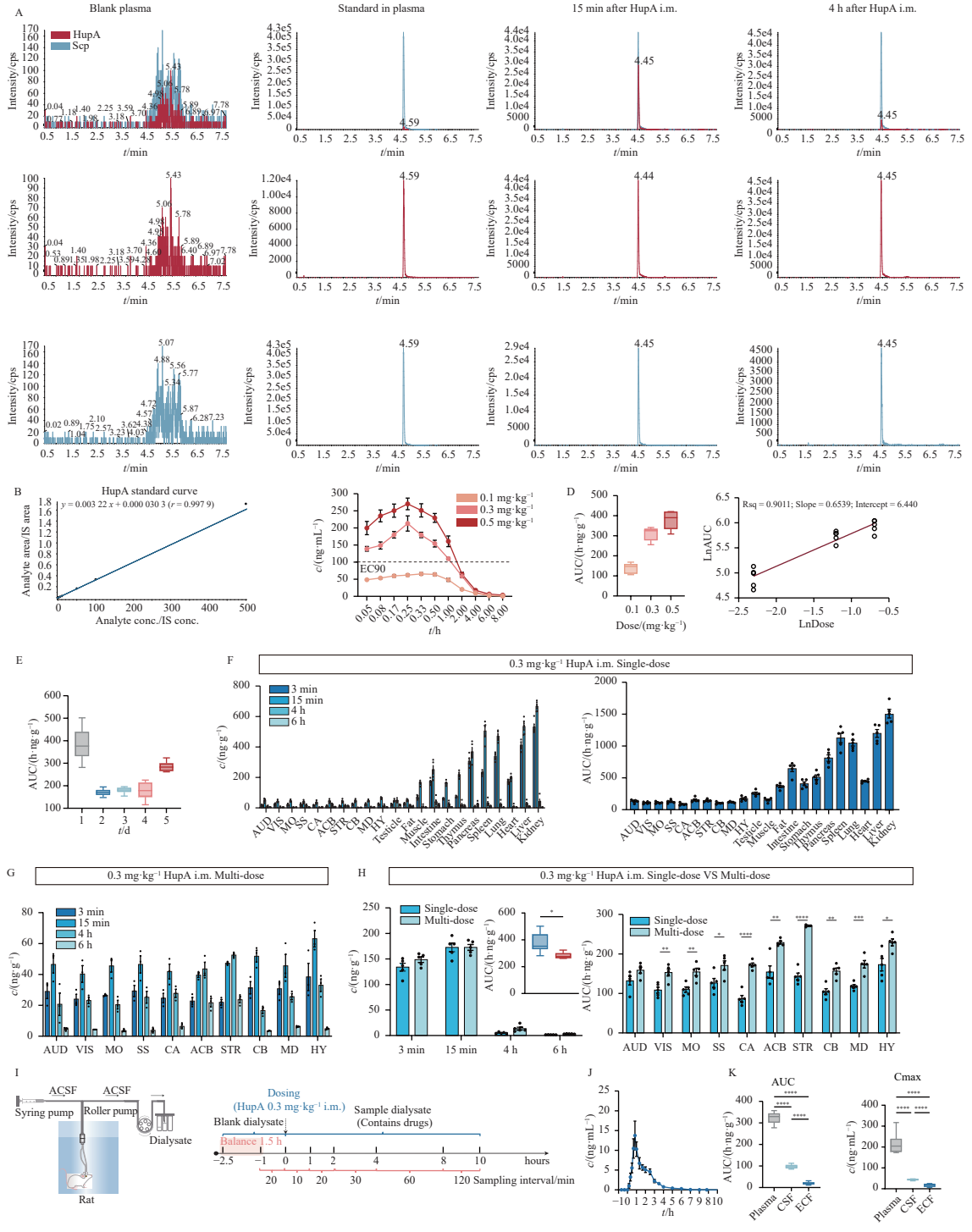

Fig. 2 Plasma pharmacokinetics and brain tissue distribution of HupA under physiological conditions. (A) Representative MRM chromatograms for HupA and IS: a blank rat plasma sample; a blank rat plasma sample spiked with HupA (100 ng·mL^{-1}) and IS (50 ng·mL^{-1}); a plasma rat sample 15 min after intramuscular injection of HupA (0.5 mg·kg^{-1}, HAI); a plasma rat sample 4 h after intramuscular injection of HupA (0.5 mg·kg^{-1}, HAI). (B) Quantitative standard curve of HupA in rat plasma from 0.5 to 500 ng·mL^{-1}. y = 0.003 22 x + 0.000 030 3 (r = 0.9979). (C) Comparison of plasma concentration-time (0.1, 0.3 and 0.5 mg·kg^{-1}) profiles of HupA with EC_{90}100.76 ng·mL^{-1} (n = 6). (D) Doses-exposure level of HupA *in vivo*; Doses-AUC linear analysis plot of HupA. (E) The drug exposure of multiple-doses day-to-day variation (n = 6). (F) Concentration (ng·g^{-1}) and AUC (h·ng·g^{-1}) in different tissues after single dose of 0.3 mg·kg^{-1} HupA (n = 6). (G) Concentration (ng·g^{-1}) in different tissues after multiple doses of 0.3 mg·kg^{-1} HupA. (H) Comparison between single and multiple dose on plasma drug concentration and AUC of 0.3 mg·kg^{-1} HupA i.m. (n = 6). (I) Schematic diagram of microdialysis sampling device with free-moving of rat; Flowchart of continuous microdialysis sampling procedure. (J) ECF concentration-time curve of 0.3 mg·kg^{-1} HupA of i.m. single dose (n = 6). (K) Differences in AUC and C_{max} across plasma, cerebrospinal fluid, and extracellular fluid (n = 6). Data represent mean ± SEM. $^{*}P$ < 0.05, $^{****}P$ < 0.0001; two-tailed unpaired Student's t-test.

imal concentration (EC_{90}) of 100.76 ng·mL^{-1}. Comparison of plasma concentration-time profiles at 0.1, 0.3, and 0.5 mg·kg^{-1} (Fig. 2C) revealed that the 0.1 mg·kg^{-1} dose resulted in concentrations consistently below the EC_{90}, whereas the 0.3 mg·kg^{-1} dose maintained concentrations above EC_{90} for approximately 1.2 h, and the 0.5 mg·kg^{-1} dose for about 1.8 h. Therefore, a dose of 0.3 mg·kg^{-1} was selected for subsequent studies to achieve sustained target engagement with minimal excess exposure.

The non-compartmental parameters for multiple-dose administration are presented in Table 6, fitted using a one-compartment model and compared with single-dose PK (Table 7). The cumulative index for HupA was 1.00 ± 0.00, indicating no accumulation upon repeated dosing. Furthermore, drug exposure on subsequent days was significantly reduced compared to day one,

Table 4 Non-compartmental pharmacokinetic parameters of HupA in plasma following intramuscular injection (n = 6 per dose group).

Dosage (mg·kg^{-1})	Ke[a] (h^{-1})	$t_{1/2}$[a] (h)	T_{max}[a] (h)	C_{max}[a] (ng·mL^{-1})	AUC_{0-t}[a] (h·ng·mL^{-1})	$AUC_{0-\infty}$[a] (h·ng·mL^{-1})	V[a] (m·kg^{-1})	Cl[a] (mL·h^{-1}·kg^{-1})	MRT_{0-t}[a] (h)	$MRT_{0-\infty}$[a] (h)	$AUMC_{0-t}$[a] (h·h·ng·mL^{-1})	$AUMC_{0-\infty}$[a] (h·h·ng·mL^{-1})
0.1	0.61 ± 0.08	1.16 ± 0.14	0.39 ± 0.13	68.12 ± 8.87	135.19 ± 20.45	136.61 ± 20.26	1256.77 ± 281.36	745.88 ± 113.19	1.61 ± 0.15	1.70 ± 0.15	219.09 ± 41.12	232.89 ± 39.71
0.3	0.63 ± 0.09	1.12 ± 0.18	0.22 ± 0.04	215.25 ± 52.35	323.99 ± 27.90	326.32 ± 28.13	1501.55 ± 280.99	925.42 ± 84.66	1.38 ± 0.13	1.44 ± 0.15	448.98 ± 67.82	471.55 ± 73.99
0.5	0.55 ± 0.14	1.34 ± 0.38	0.25 ± 0.05	273.15 ± 43.83	443.79 ± 60.45	452.06 ± 64.59	2169.81 ± 667.15	1123.17 ± 144.85	1.40 ± 0.33	1.55 ± 0.50	625.87 ± 196.29	711.59 ± 290.52

The mean concentration–time profiles from different animals at each time point were used to estimate the pharmacokinetic parameters. [a]Ke, elimination rate constant; $t_{1/2}$, elimination half-time; T_{max}, time to reach maximum concentration; C_{max}, maximum concentration; AUC_{0-t}, area under the curve from time 0 to time t; $AUC_{0-\infty}$, area under the curve from time 0 to infinity; V, volume of distribution; Cl, Clearance; MRT_{0-t}, mean residence time from time 0 to time t; $MRT_{0-\infty}$, mean residence time from time 0 to infinity; $AUMC_{0-t}$, area under the moment curve from time 0 to time t; $AUMC_{0-\infty}$, area under the moment curve from time 0 to infinity. [b]$MRT_{0-t} = \frac{AUC_{0-t}}{AUMC_{0-t}}$ $MRT_{0-\infty} = \frac{AUC_{0-\infty}}{AUMC_{0-\infty}}$

Table 5 Pharmacokinetic parameters of HupA in plasma fitted with a one-compartment model (1/C weighting) (n = 6 per group).

Dosage (mg·kg^{-1})	K_{01} (h^{-1})[a]	K_{10} (h^{-1})[a]	V_F (mL·kg^{-1})[a]	AUC (h·ng·mL^{-1})[a]	CL_F (mL·h^{-1}·kg^{-1})[a]	C_{max} (ng·mL^{-1})	T_{max} (h)	$t_{1/2}$ (h)	K_{01-HL} (h^{-1})[a]	K_{10-HL} (h^{-1})[a]
0.1	19.44 ± 7.40	0.56 ± 0.09	1352.00 ± 198.03	135.71 ± 23.567	756.03 ± 132.17	66.88 ± 8.14	0.20 ± 0.06	1.82 ± 0.30	0.04 ± 0.02	1.26 ± 0.21
0.3	17.22 ± 4.24	0.74 ± 0.13	1355.90 ± 185.99	308.01 ± 29.00	981.93 ± 1101.59	194.00 ± 21.72	0.20 ± 0.03	1.39 ± 0.24	0.04 ± 0.01	0.97 ± 0.16
0.5	20.74 ± 6.15	0.73 ± 0.19	1668.10 ± 366.28	433.92 ± 75.17	1177.29 ± 175.29	272.23 ± 45.97	0.18 ± 0.04	1.45 ± 0.42	0.04 ± 0.01	1.01 ± 0.29

[a]K_{01}, absorption rate constant; K_{10}, elimination rate constant; V_F, apparent volume of distribution adjusted by bioavailability; AUC, area under the curve; CL_F, apparent clearance adjusted by bioavailability.

Table 6 Non-compartmental pharmacokinetic parameters of HupA in plasma after a single 0.3 mg·kg^{-1} intramuscular injection in healthy rats (n = 6 per group).

Subject	Accumulation index	AUC_Tau (h·ng·mL^{-1})	C_avg (ng·mL^{-1})	Fluctuation%	AUC_M Tau (h·h·ng·mL^{-1})
normal rats	1.00 ± 0.00	293.04 ± 23.61	12.21 ± 0.98	1476.48 ± 196.29	361.59 ± 90.77

AUC_Tau, area under the concentration-time curve over a dosing interval; C_avg, average concentration; AUC_M Tau, area under the AUC over a dosing interval (τ\tau), adjusted for the drug's half-life.

Table 7 Non-compartmental pharmacokinetic parameters of HupA in plasma following 0.3 mg·kg^{-1} intramuscular administration in healthy and MCAO rats (n = 6 per group).

Subject	Ke (h^{-1})	$t_{1/2}$ (h)	T_{max} (h)	C_{max} (ng·mL^{-1})	AUC_{0-t} (h·ng·mL^{-1})	$AUC_{0-\infty}$ (h·ng·mL^{-1})	V (mL·kg^{-1})	Cl (mL·h·kg^{-1})	MRT_{0-t} (h)	$MRT_{0-\infty}$ (h)	$AUMC_{0-t}$ (h·h·ng·mL^{-1})	$AUMC_{0-\infty}$ (h·h·ng·mL^{-1})
Single-dosing	0.54 ± 0.09	1.31 ± 0.24	0.29 ± 0.07	194.81 ± 18.67	375.90 ± 75.46	380.87 ± 78.07	1549.11 ± 461.05	814.17 ± 158.45	1.45 ± 0.15	1.55 ± 0.19	554.44 ± 174.53	603.70 ± 200.82
Multiple-dosing	0.67 ± 0.10	1.06 ± 0.16	0.32 ± 0.11	178.76 ± 12.50	282.49 ± 22.85	284.66 ± 22.84	1567.23 ± 226.99	——	——	0.54 ± 0.19	——	——

while no notable changes were observed in half-life or other key PK parameters. The AUC during multiple dosing was 75.15% of the AUC observed after single dosing (Fig. 2E). Collectively, these findings demonstrate that HupA exhibits linear PK and does not accumulate with repeated administration.

3.2. Brain distribution of HupA in rats under single and multiple dosing regimens

We further evaluated the tissue distribution of HupA following single and multiple intramuscular administrations in normal rats. After a single dose, HupA concentrations were markedly elevated in the liver, kidney, spleen, lung, and pancreas, whereas brain levels remained relatively low (Fig. 2F). Drug exposure was highest in the kidney (1507.25 ± 152.34 h·ng·g^{-1}), followed by the spleen, lung, pancreas, intestine, thymus, heart, stomach, muscle, testes, fat, and brain, with hippocampal exposure measured at 93.03 ± 18.83 h·ng·g^{-1} (Fig. 2F). To assess regional brain exposure after repeated administration, we determined HupA levels across different brain regions. Following multiple doses, drug exposure increased in all brain regions, while plasma concentrations declined concomitantly (Fig. 2G). A comparative analysis of AUC values between single and multiple dosing revealed that repeated administration enhanced HupA penetration into brain tissue, potentially augmenting its pharmacological activity (Fig. 2H).

To further investigate the brain kinetics of HupA and achieve sufficient temporal resolution for subsequent mPBPK-PD modeling, microdialysis was employed to continuously collect ECF from the CA1 region of the Hc in freely moving rats (AP: −4.8 mm, ML: −5.0 mm, DV: −5.0 mm) (Fig. 2I). An analytical method for quantifying HupA in ECF was developed, demonstrating a linear range of 0.5–1000 ng·mL^{-1} (r = 0.9946) and an LLOQ of 0.5 ng·mL^{-1}, indicating high sensitivity. The concentration-time profile of HupA in ECF is shown in Fig. 2J. Following a single intramuscular injection (0.3 mg·kg^{-1}), T_{max} in the brain was 0.92 h, significantly later than the peak time observed in plasma.

We examined HupA concentrations in CSF and arterial blood after administration. Comparative analysis of C_{max} and AUC ratios indicated that a substantial proportion of HupA enters the central CSF from peripheral arterial blood, with a calculated brain penetration rate of 39.03%. This suggests efficient BBB permeability, which is favorable for treating CNS disorders. A differential analysis of C_{max} and AUC ratios among arterial blood, CSF, and ECF was conducted (Fig. 2K). The results revealed a marked reduction in HupA exposure along the transfer pathway, implying that the drug requires a finite transit time to cross both the BBB and the blood-cerebrospinal fluid barrier (BCSFB) before reaching the CSF and ECF, contributing to the delayed C_{max}.

3.3. Effects of HupA on ACh and other neurotransmitters in the brain.

As an AChE inhibitor, the therapeutic efficacy of HupA primarily depends on its modulation of central and peripheral ACh levels. Previous studies have demonstrated that ACh mediates anti-inflammatory responses and enhances neural function

via α7nAChRs and α4β2nAChRs [33, 34]. Therefore, ACh was selected as the primary PD biomarker for HupA modeling. Using LC-MS/MS, we established a quantitative method for analyzing neurotransmitters in brain tissue and ECF, with detailed mass spectrometry parameters provided in Table 1. ACh concentrations were measured in various brain regions after single and multiple administrations of HupA (0.3 mg·kg^{-1}) and subjected to correlation analysis (Figs. 3A–3D). The results showed a strong correlation between HupA concentrations and ACh levels, particularly in the medulla oblongata (MO). Notably, ACh levels were highest in the Hc and striatum (STR), and repeated dosing led to a significant increase in the temporal lobe, suggesting region-specific pharmacological relevance.

In addition, we profiled changes in several other neurotransmitters, Adr, Aspa, NE, DA, γ-GABA, Glu, 5-HT, and 5-HIAA, across these brain regions. Following HupA administration, monoamine neurotransmitter levels (Adr, NE, DA) and Aspa increased, whereas Glu and 5-HT decreased. GABA and 5-HIAA levels decreased after a single dose but increased following multiple administrations (Figs. 4A–4B). Subsequently, dynamic changes in neurotransmitter levels within the hippocampal CA1 ECF were monitored after a single dose (Fig. 4C). ACh levels rose and remained elevated for approximately 8 h before returning to baseline. Adr peaked at around 6 h, while NE and Aspa concentrations remained elevated for over 10 h. Glu levels were reduced for more than 10 h, and 5-HIAA levels were elevated for about 10 h. No statistically significant alterations were observed in extracellular 5-HT, DA, or GABA levels post-administration. Correlation analysis between neurotransmitter changes and HupA concentration was performed (Fig. 4D). ACh and Adr exhibited statistically significant but moderate correlations with HupA concentration ($P < 0.0001$; $r = 0.4267$ and 0.4213, respectively), indicating potential involvement in HupA's pharmacological effects.

3.4. PK and brain distribution of HupA in MCAO-related pathological states

To explore the relationship between HupA and ACh dynamics under pathological conditions, a rat model of MCAO was established (Fig. 5A). Dual-wavelength laser Doppler flowmetry confirmed that cerebral blood flow decreased to 57.6% ± 5.2% of baseline (100%) following filament insertion, indicating significant hypoperfusion, particularly in the right cerebral cortex (Fig. 5B). After 2 h of ischemia, blood flow partially recovered to 73.2% ± 6.4%, confirming successful reperfusion (Fig. 5C). Twenty-four hours after ischemia and 2 h of reperfusion, brain sections were stained with 1% TTC to evaluate cerebral infarction. The infarct area was significantly larger in the MCAO group compared to the sham group, averaging 24.24% ± 0.25% (Figs. 5D and 5E). Neurological function was assessed using the Longa scoring method in seven randomly selected rats per group. Additionally, brain water content in the ischemic hemisphere was significantly higher than in the non-ischemic hemisphere and the sham group (80.77% ± 0.55% *vs.* 76.00% ± 0.97%), indicating pronounced edema in the affected region (Fig. 5F). Neurological deficits were significantly greater in the MCAO group (Longa

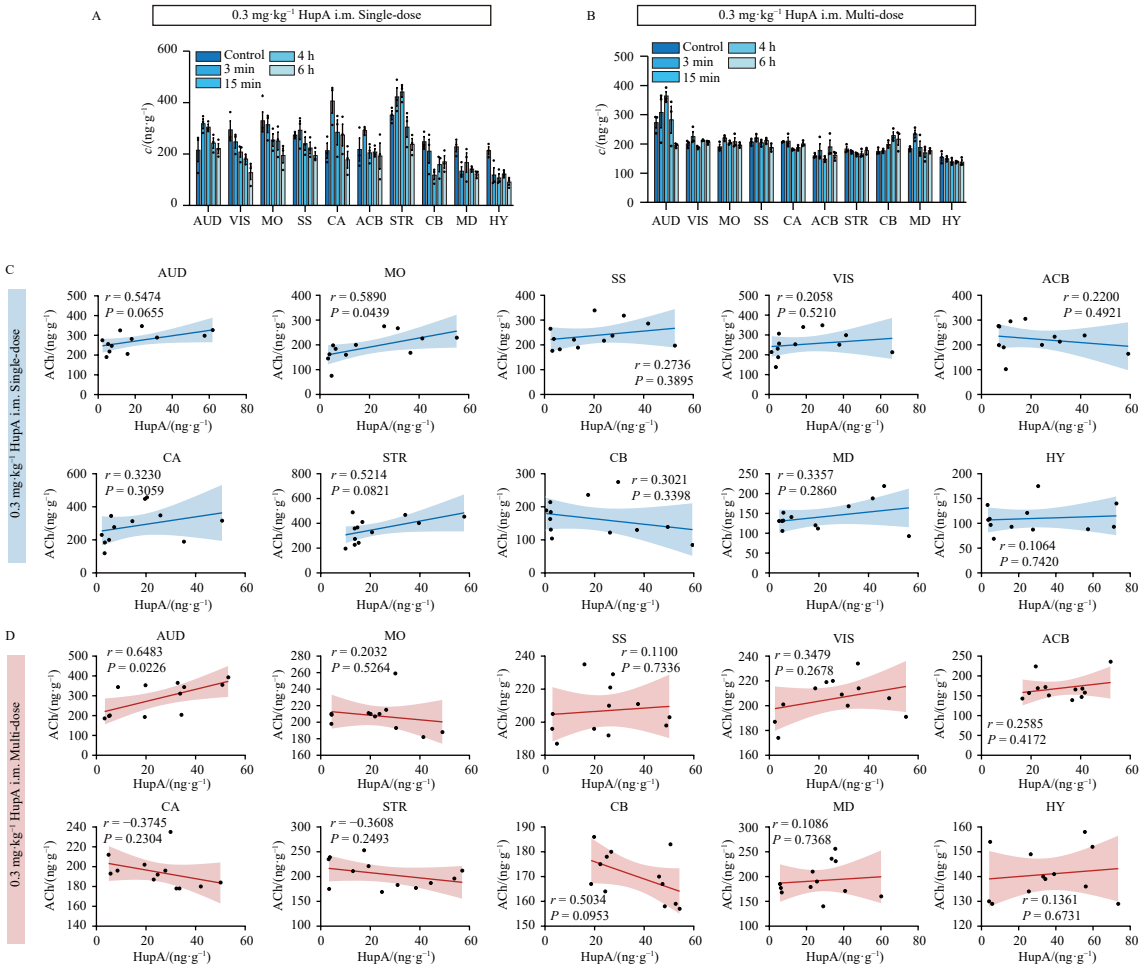

Fig. 3 Correlation between ACh levels and HupA concentrations in normal rats. Changes in ACh concentration after a single dose (A) and multiple doses (B) of 0.3 mg·kg^{-1} HupA administered intramuscularly in various brain regions of rats ($n = 3$). Correlation analysis of HupA and ACh concentrations in the brain after a single dose (C) and multiple doses (D) of 0.3 mg·kg^{-1} HupA ($n = 3$). Data represent mean ± SEM.

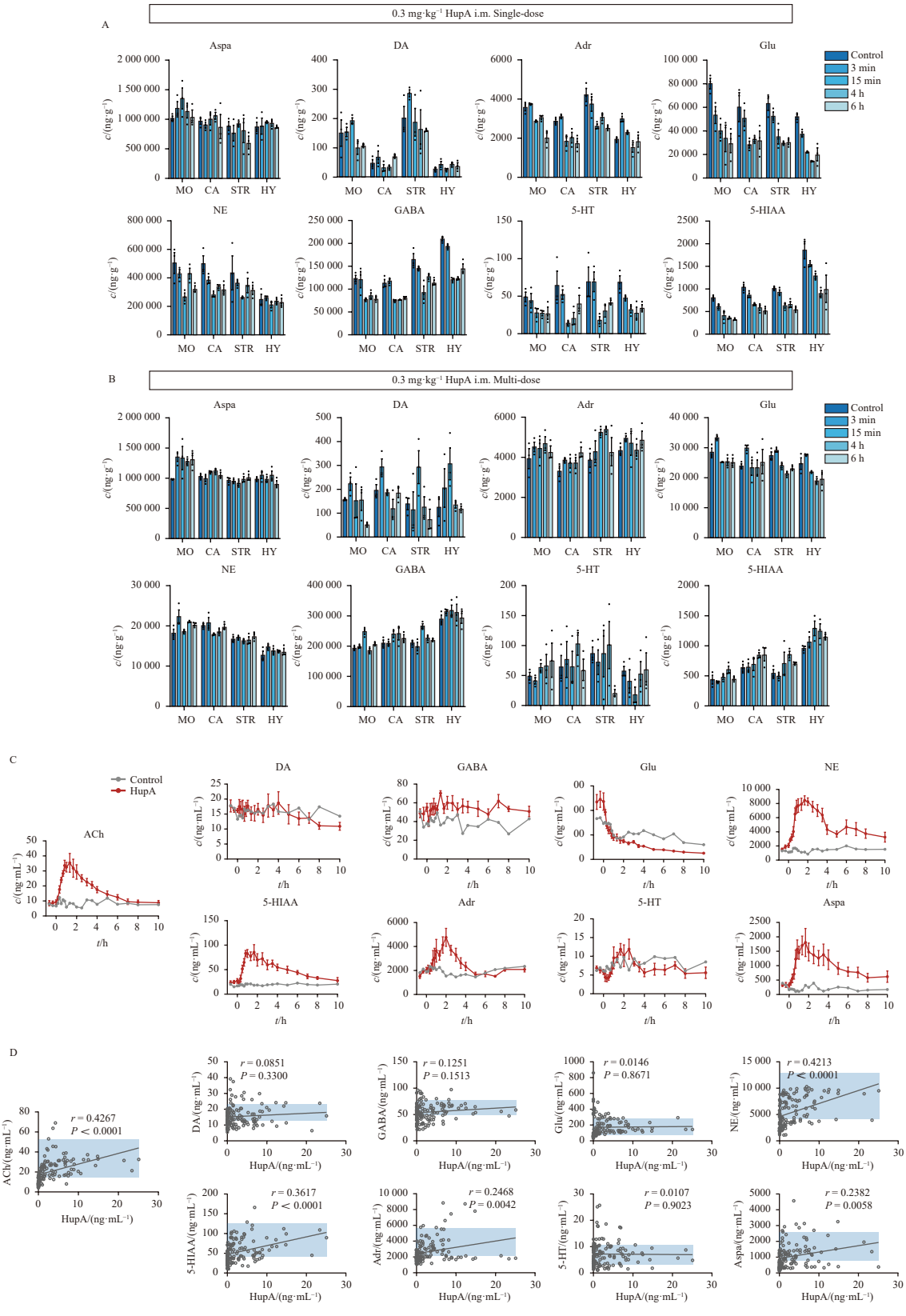

Fig. 4 Effects of HupA on neurotransmitter levels in normal rat brain. Changes in different neurotransmitters after single (A) and multiple (B) administrations in rats (n = 3). (C) Changes in ECF neurotransmitter concentration in the presence and absence of HupA administration (n = 7). (D) Correlation analysis of HupA and neurotransmitters in ECF. $^{*}P < 0.05$, $^{**}P < 0.01$, $^{***}P < 0.001$, calculated using two-way repeated measures analysis of variance (ANOVA). Data are presented as mean ± SEM.

score: 2.78 ± 0.15) compared to the sham group (Fig. 5G). Compared to the untreated MCAO model, HupA treatment reduced cortical infarct volume (Fig. 5H) and improved survival (Fig. 5I). However, no significant differences were observed in body weight or neurological deficit scores (Figs. 5J and 5K)

Next, we investigated the PK characteristics of HupA in the MCAO model (Fig. 6A). Blood samples were collected at sequential time points following intramuscular administration of

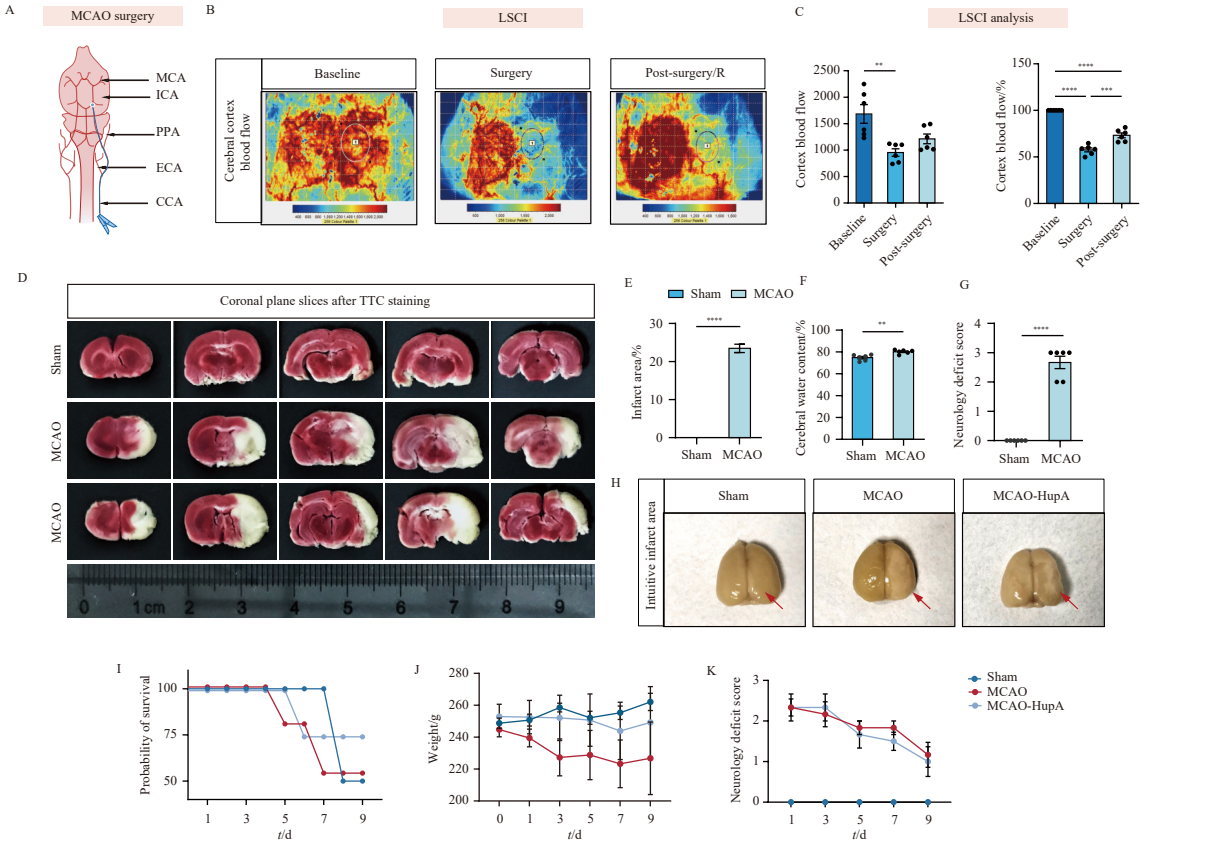

Fig. 5 Establishment of Middle Cerebral Artery Occlusion rat model. (A) Schematic of embolization in MCAO model. (B) Real-time monitoring of cortical blood flow with laser speckle contrast imaging before surgery (baseline), during embolization, and post-surgery (reperfusion) in the MCAO model (n = 6). (C) Comparison of blood flow reduction after embolization with baseline levels for analysis. (D) Representative images of TTC staining. Quantitative analysis of cerebral infarct area (E), water content (F) and neurology deficit score (Longa scoring, G) in MCAO and Sham rats (n = 6). (H) Intuitive infarct Area of the cerebral cortex (n = 6). (I) Probability of survival after HupA dose. Probability of survival = (Number of rats surviving on the day)/(Total number of rats on the day). (J) Body weight changes and Longa scoring in rats after HupA administration (n = 6). (K) Neurological deficit score during 9 days (n = 6). $^{**}P < 0.01$, $^{***}P < 0.001$, $^{****}P < 0.0001$, calculated using two-tailed unpaired Student's t-test. Data are presented as mean ± SEM.

0.3 mg·kg^{-1} HupA to MCAO rats, and the resulting plasma concentration-time curve is presented in Fig. 6B. Single-dose PK analysis was performed using a one-compartment model in Phoenix WinNonlin, with model selection based on weighted residual sum of squares, AIC, and BIC (Tables 8 and 9). Results indicated that HupA follows first-order elimination kinetics, with plasma concentration declining exponentially over time.

For multiple dosing, PK parameters were fitted using a one-compartment model under the same criteria (Table 10). The accumulation ratio was 1.03 ± 0.03, indicating minimal drug accumulation. However, comparison of C_{max} and AUC revealed that the AUC after multiple dosing was 162.22% of the single-dose value, while C_{max} was 92.12% (Table 11), suggesting a notable increase in systemic exposure (Fig. 6C). The $t_{1/2}$ of HupA was slightly prolonged after a single dose in MCAO rats (1.23 ± 0.16 h) compared to normal rats (1.12 ± 0.18 h). With multiple dosing, the half-life extended nearly threefold (3.84 ± 1.85 h), likely due to impaired metabolism and clearance in the ischemic state, leading to sustained plasma concentrations.

The plasma concentration and brain region distribution of HupA following multiple intramuscular injections (0.1 mg·kg^{-1}) are illustrated in Fig. 6D. HupA exhibited linear PK behavior, with dose-normalized AUC used to compare drug exposure across brain regions after single and multiple administrations in both normal and pathological states (Fig. 6E). We further analyzed ACh concentrations in various brain regions of MCAO rats and assessed the correlation between ACh and HupA levels in each region (Figs. 6F and 6G). A strong correlation was observed between HupA concentration and ACh changes in the STR under MCAO conditions, whereas hippocampal ACh levels significantly decreased, consistent with patterns associated with cognitive impairment.

3.5. Effects of HupA on ACh and other neurotransmitters under pathological conditions

We further evaluated neurotransmitter dynamics in different brain regions of the MCAO rat model, including ACh, 5-HT, 5-HIAA, DA, NE, Adr, GABA, Glu, and Aspa (Figs. 7A–7C). After a single administration, measurements taken at 6 h (Fig. 7A) revealed that HupA reduced Adr and Aspa concentrations in the STR, with no significant changes in other neurotransmitters. Following six days of administration, more pronounced effects emerged: ACh, NE, DA, Aspa, GABA, and 5-HIAA levels increased, while Glu, Adr, and 5-HT decreased (Fig. 7B). After a three-day withdrawal period, the HupA-treated group exhibited reduced ACh, NE, and DA levels in the MO (Fig. 7C). These findings, combined with data from normal physiological conditions, indicate that HupA modulates neurotransmitter dynamics in a time- and region-dependent manner.

3.6. Establishment and validation of an mPBPK-PD model

Based on the previously obtained single- and multiple-dose PK data, we initially predicted daily dosing frequency and corresponding blood concentration profiles using Phoenix WinNonlin 8.3 (Fig. 8A). In the MCAO rat model, predicted plasma concentrations after multiple dosing closely matched observed values, with nearly all data points falling within the 90% confidence interval (Fig. 8B).

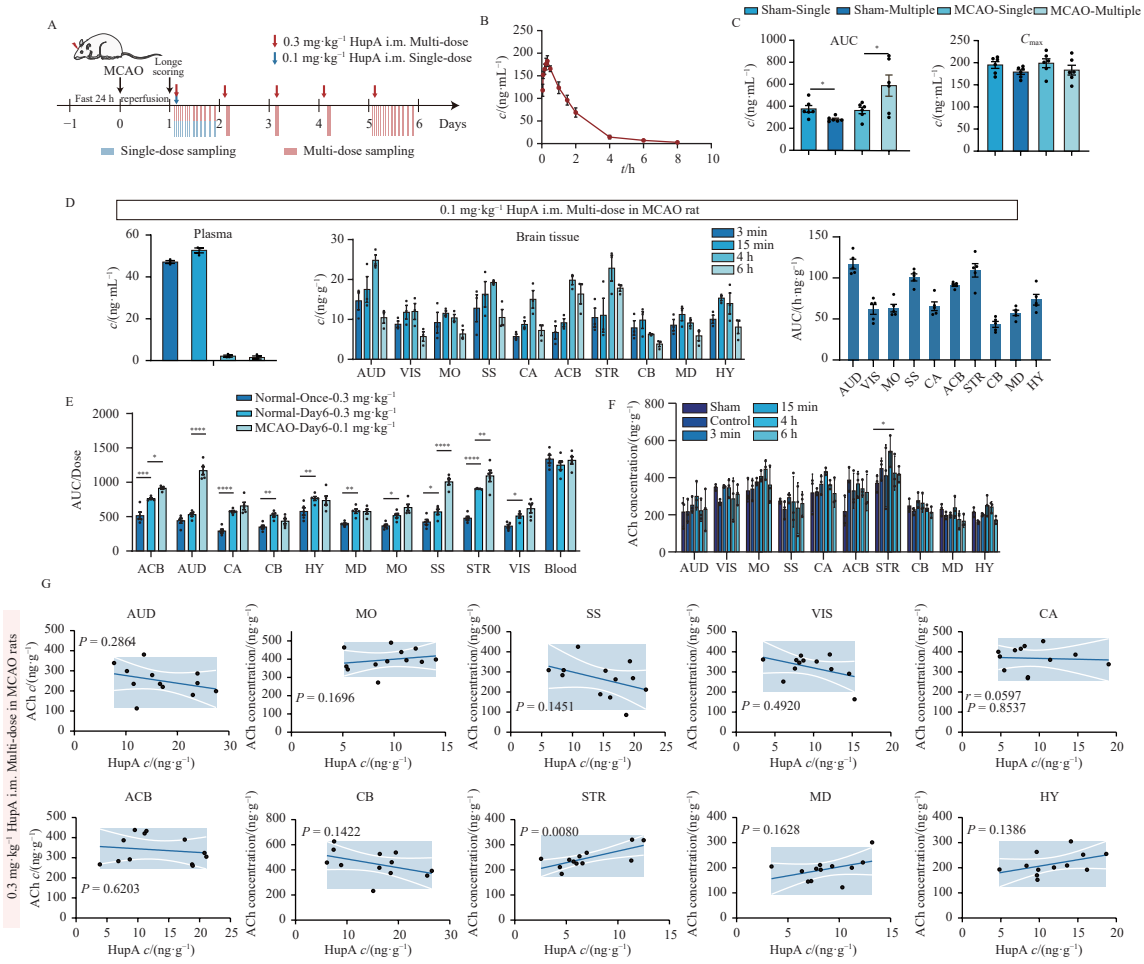

Fig. 6 Pharmacokinetic behavior of HupA and the alterations of ACh in MCAO rat. (A) Experimental-procedure workflow of the MCAO modeling and sampling. (B) Concentration-time curve of plasma after HupA injection of 0.3 mg·kg^{-1} on MCAO intramuscularly (n = 6). (C) AUC and C_{max} comparisons between MCAO (single/multiple doses) and normal rats (single/multiple doses) (n = 6). (D) Drug distribution of HupA in plasma and tissues following administration in the MCAO model (n = 3). (E) Distribution of HupA in relevant brain tissues after single and multiple dose of 0.3 mg·kg^{-1} (i.m.) in physiological conditions, and after single dose (i.m.) of 0.1 mg·kg^{-1} in the pathological state of MCAO, normalized using AUC/Dose. (F) Changes in ACh concentration after a single dose of 0.3 mg·kg^{-1} HupA administered intramuscularly in various brain regions in Sham and MCAO rats (n = 3). (G) Correlation analysis of HupA and ACh concentrations in the brain after multiple doses of 0.3 mg·kg^{-1} HupA in MCAO rats (n = 3). Data represent mean ± SEM. $^{*}P < 0.05$, $^{**}P < 0.01$, $^{***}P < 0.001$, $^{****}P < 0.0001$; two-tailed unpaired Student's t-test, except for (G) (one-way ANOVA with Tukey's post-hoc test).

Table 8 Comparative non-compartmental analysis of HupA pharmacokinetics in plasma after 0.3 mg·kg^{-1} intramuscular injection between healthy and middle cerebral artery occlusion (MCAO) model rats (n = 6 per group).

Subject	Ke (h^{-1})	$t_{1/2}$ (h)	T_{max} (h)	C_{max} (ng·mL^{-1})	AUC_{0-t} (h·ng·mL^{-1})	$AUC_{0-\infty}$ (h·ng·mL^{-1})	V (mL·kg^{-1})	Cl (mL·h^{-1}·kg^{-1})	MRT_{0-t} (hr)	$MRT_{0-\infty}$ (h)	$AUMC_{0-t}$ (h·h·ng·mL^{-1})	$AUMC_{0-\infty}$ (h·h·ng·mL^{-1})
normal rats	0.63 ± 0.09	1.12 ± 0.18	0.22 ± 0.04	215.25 ± 52.35	323.97 ± 27.90	326.29 ± 28.13	1501.60 ± 281.01	925.48 ± 84.66	1.38 ± 0.13	1.44 ± 0.15	448.98 ± 67.82	471.55 ± 73.99
MCAO rats	0.57 ± 0.07	1.23 ± 0.16	0.36 ± 0.11	198.83 ± 24.29	362.33 ± 71.71	367.60 ± 72.89	1498.22 ± 361.20	850.38 ± 210.27	1.57 ± 0.21	1.68 ± 0.26	572.60 ± 145.82	624.70 ± 168.47

Table 9 One-compartment model parameters of HupA in plasma with 1/C weighting.

Subject	$K01$ (h^{-1})	$K10$ (h^{-1})	V_F (mL·kg^{-1})	AUC (h·ng·mL^{-1})	CL_F (mL·h^{-1}·kg^{-1})	C_{max} (ng·mL^{-1})	T_{max} (h)	$t_{1/2}$ (h)	$K_{01\text{-}HL}$ (h^{-1})	$K_{10\text{-}HL}$ (h^{-1})
normal rats	17.46 ± 4.72	0.73 ± 0.13	1359.14 ± 189.46	308.78 ± 29.19	979.59 ± 102.18	193.80 ± 21.85	0.20 ± 0.03	1.40 ± 0.24	0.04 ± 0.01	0.97 ± 0.17
MCAO Rats	17.13 ± 4.05	0.59 ± 0.14	1465.17 ± 168.59	371.63 ± 100.14	861.51 ± 246.65	182.73 ± 19.67	0.21 ± 0.04	1.79 ± 0.42	0.04 ± 0.01	1.24 ± 0.29

Table 10 Non-compartmental pharmacokinetic parameters of HupA in plasma after 5-day repeated 0.3 mg·kg^{-1} intramuscular injections in MCAO rats (n = 6 per group).

Subject	Accumulation index	AUC_Tau (h·ng·mL^{-1})	C_{avg} (ng·mL^{-1})	Fluctuation%	AUC_M Tau (h·h·ng·mL^{-1})
MCAO Rats	1.03 ± 0.03	599.22 ± 221.37	24.97 ± 9.22	805.46 ± 246.16	2125.61 ± 1134.67

Table 11 Non-compartmental pharmacokinetic parameters of HupA in plasma following single and multiple 0.3 mg·kg^{-1} intramuscular injections in MCAO rats (n = 6 per group).

Subject	Ke (h^{-1})	$t_{1/2}$ (h)	T_{max} (h)	C_{max} (ng·mL^{-1})	AUC_{0-t} (h·ng·mL^{-1})	$AUC_{0-\infty}$ (h·ng·mL^{-1})	V (mL·kg^{-1})	Cl (mL·h^{-1}·kg^{-1})	MRT_{0-t} (h)	$MRT_{0-\infty}$ (h)	$AUMC_{0-t}$ (h·h·ng·mL^{-1})	$AUMC_{0-\infty}$ (h·h·ng·mL^{-1})
Single-dosing	0.57 ± 0.07	1.23 ± 0.16	0.36 ± 0.11	198.83 ± 24.29	362.33 ± 71.71	367.60 ± 72.89	1498.22 ± 361.20	850.38 ± 210.27	1.57 ± 0.21	1.68 ± 0.26	572.60 ± 145.82	624.70 ± 168.47
Multiple-dosing	0.23 ± 0.13	3.84 ± 1.85	0.42 ± 0.13	183.17 ± 27.00	587.76 ± 237.04	600.30 ± 238.62	2746.01 ± 926.67	——	——	3.10 ± 1.88	——	——

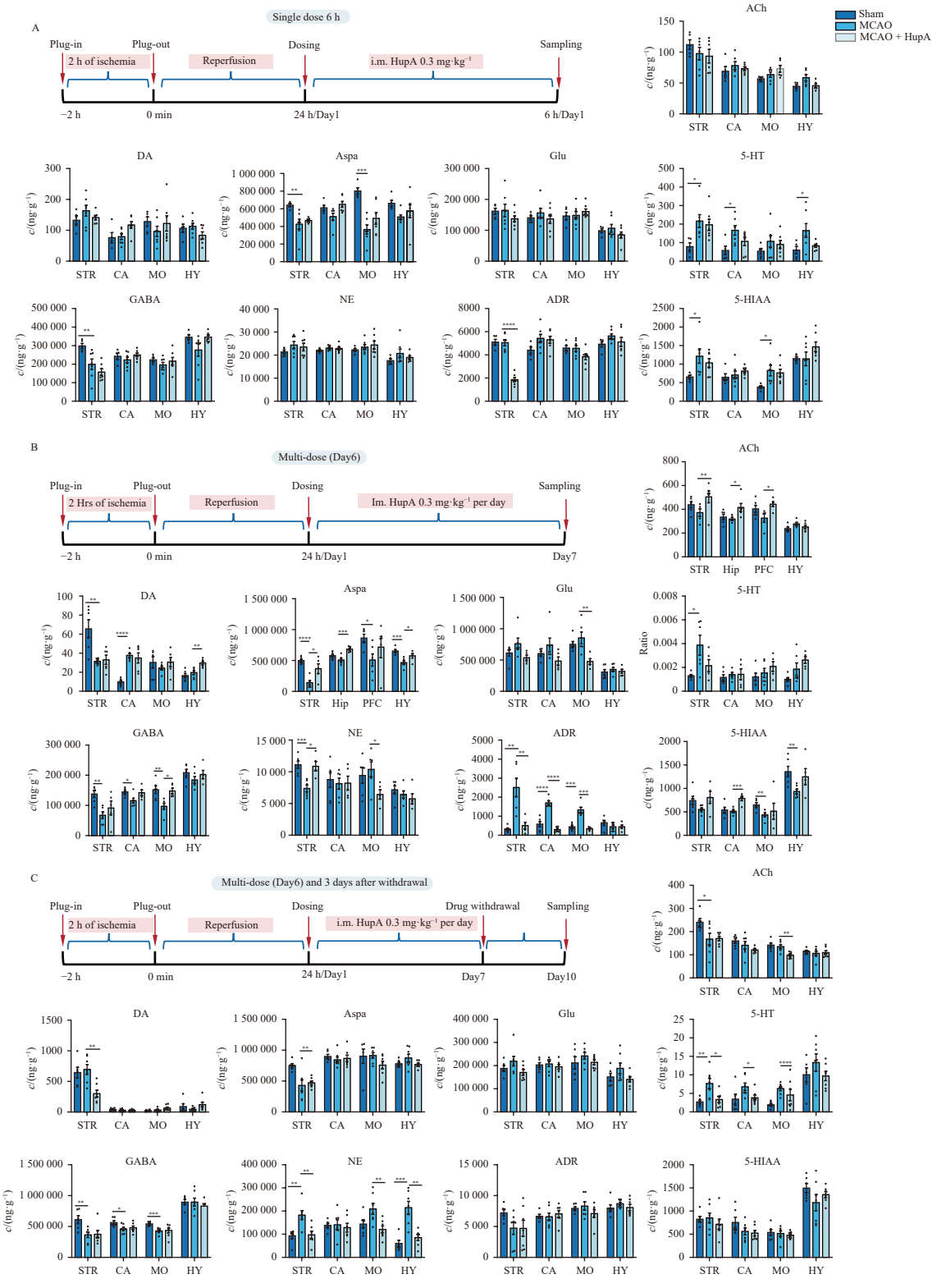

Fig. 7 Impact of HupA on multiple neurotransmitters in the MCAO rat. (A) Experimental scheme of single-dose HupA treatment in MCAO model; Concentration of neurotransmitters in related brain regions after single-dose treatment. (B) Experimental scheme of multi-dose HupA treatment in MCAO model; Concentration of neurotransmitters in related brain regions after multi-dose treatment. (C) Experimental scheme of drug withdrawal effect in multi-dose HupA treatment in MCAO model; Concentration of neurotransmitters in related brain regions after drug withdrawal. Data represent mean ± SEM (n = 7). $^{*}P < 0.05$, $^{**}P < 0.01$, $^{***}P < 0.001$, $^{****}P < 0.0001$; two-tailed unpaired Student's t-test.

HupA undergoes relatively rapid metabolism following intramuscular injection. If only metabolic clearance was considered, maintaining therapeutic efficacy would necessitate 4–6 daily doses. However, considering the prolonged time-course of ACh elevation, a key PD marker, we observed that the pharmacological effects of HupA persist longer than the drug's presence in circulation. Given that ACh is a critical neurotransmitter involved in widespread physiological functions and strongly linked to cognitive enhancement and other therapeutic actions [35], dosing regimen design should integrate PD target dynamics alongside PK data. As a well-established biomarker, ACh has been extensively studied for its utility in disease detection methods [36, 37]

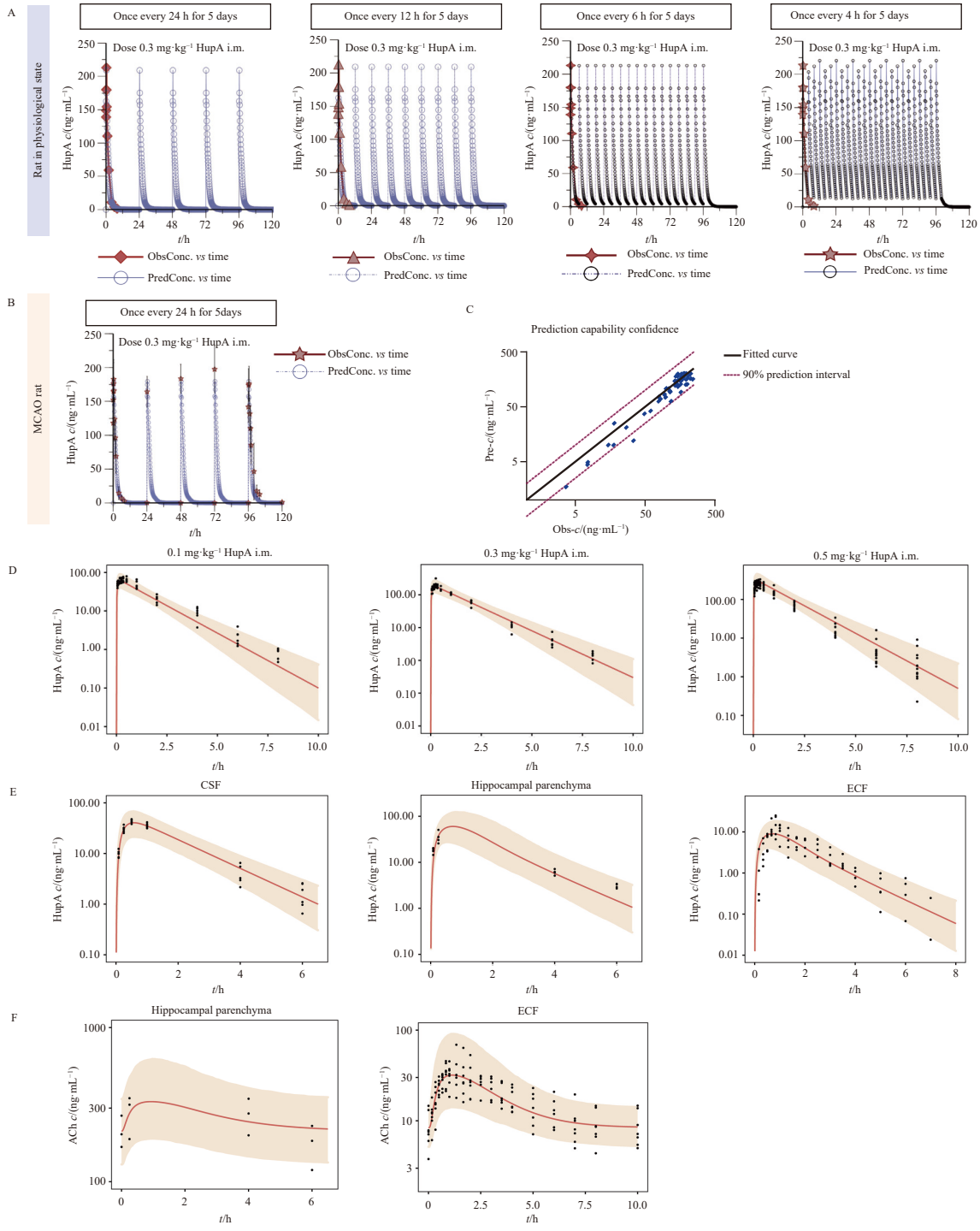

Fig. 8 Establishment and validation of the mPBPK-PD model. (A) Prediction of HupA concentration in plasma changes after multiple dosing based on single-dose data. (B) Single administration predicts HupA concentrations changes in plasma for multiple administrations in MCAO rats. Data was performed using Phoenix WinNonlin 8.3 software. (C) 90% prediction confidence interval for the prediction of HupA in MCAO rats. (D) Visual predictive check (VPC) plots for the PK model-predicted concentration of 0.1, 0.3 and 0.5 mg·kg^{-1} HupA intramuscular in rat plasma over time. (E) VPC plots for the predicted value of HupA concentration in rat CSF, hippocampal parenchyma and ECF *via* PK model over time. (F) VPC plots for the predicted value of ACh concentration in rat ECF and hippocampal parenchyma of rats *via* PK model over time. Black dots: observed values; orange solid line: population predictions; orange shaded area: 90% confidence interval of predicted values.

Building upon the HupA PK model, we constructed a mechanistic PBPK-PD (mPBPK-PD) model using hippocampal and ECF ACh concentrations as PD endpoints (Fig. 1). Model parameters were optimized using the SAEM algorithm in Monolix Suite, resulting in excellent agreement between predicted and observed values (Fig. 8C). The model accurately predicted plasma concentration-time profiles of HupA across different doses (Fig. 8D) and successfully simulated drug concentrations in hippocampal parenchyma, CSF, and CA1 ECF (Fig. 8E).

In the PD component, a kin/kout (indirect response) model was applied to describe ACh dynamics in the Hc and interstitial fluid. Under HupA influence, ACh degradation in the Hc is inhibited, leading to increased ACh levels, which subsequently diffuse into the interstitial space. Following parameter optimization with the SAEM algorithm, the model effectively predicted time-dependent changes in ACh concentrations in both hippocampal parenchyma and CA1 ECF, showing close alignment with empirical data (Fig. 8F). After visual predictive check (VPC) and parameter refinement, all relative standard error (RSE) values were below 30%, and observed data fell within the 90% prediction interval.

The final model successfully captured the temporal profiles of HupA in plasma, hippocampal tissue, CSF, and ECF across dosing regimens and accurately predicted ACh PD responses.

4. Discussion

Traditional Chinese medicine plays an important role in the clinical treatment of cognitive impairment for various reasons [38-40]. HupA injection is clinically used for the treatment of benign memory disorders and myasthenia gravis and has also shown potential in treating other neurological diseases [6, 10, 41–42]. However, the PK behavior of HupA and its relationship with neurotransmitter dynamics and PD effects remain insufficiently characterized, particularly critical for CNS drugs, where maintaining optimal levels of ACh and other neurotransmitters in the brain is essential for maximizing therapeutic efficacy and ensuring safety. In this study, we investigated the PK-PD characteristics of HupA in rats under both physiological and pathological conditions and established an mPBPK-PD model to address these unmet needs.

First, a rapid and highly sensitive method was developed to quantify HupA in plasma, tissues, CSF, and dialysate samples using LC-MS/MS. Plasma and tissue samples were processed *via* methanol-based protein precipitation, enabling accurate measurement of HupA within a linear range of 0.5–500 ng·mL^{-1}, with a LLOQ of 0.5 ng·mL^{-1}. PK studies following single and multiple doses administered *via* intramuscular injection revealed that HupA exhibits rapid elimination, with a half-life of approximately 1.10 h. Detailed investigations indicate that HupA is primarily excreted unchanged by the kidneys and is not significantly metabolized by the liver, suggesting a low potential for clinically relevant drug interactions when co-administered with cytochrome P450 (CYP)-metabolized agents [43]. A relatively rapid clearance, allowing complete elimination within one day, has also been observed in human trials [44]. By modifying formulation strategies, including the design of nanoparticle-based drug carriers, brain-targeted delivery of HupA can be enhanced and its half-life prolonged [16]. The PK profile of HupA follows a one-compartment model with linear kinetics. Based on *in vitro* cholinesterase inhibition assays, an EC90 value was estimated, indicating that a dose of 0.1 mg·kg^{-1} does not achieve therapeutic concentrations. Furthermore, HupA exhibits a narrow therapeutic window, as a dose of 0.5 mg·kg^{-1} induced mild adverse effects such as seizures and salivation in experimental animals. Under multiple-dose regimens, no systemic accumulation of HupA was observed, and plasma exposure significantly decreased, whereas other PK parameters, including half-life, remained largely unchanged. This suggests increased tissue retention despite reduced systemic availability.

Tissue distribution following intramuscular administration of HupA was evaluated, revealing predominant localization in high-perfusion organs. Notably, although plasma drug exposure declined with repeated dosing, brain exposure increased across several regions, particularly in the Hc, STR, MO, and cortex. This enhanced cerebral retention is likely attributable to the small molecular size and high BBB permeability of HupA, supporting substantial CNS penetration and retention. The correlation between cholinergic activity in these brain regions and neurofunctional regulation under disease states [45-47], combined with our PK data, provides key insights into the pharmacological mechanism of HupA and supports its targeted action in cognitive and neuromuscular disorders.

Traditional tissue sampling methods often fail to fully exclude blood interference, leading to inaccurate measurements. To address this limitation, microdialysis technology was incorporated, offering minimal surgical impact and enabling continuous sampling, thereby providing a more accurate reflection of metabolic conditions in animals under normal physiological states [48-50]. Using this technique, we continuously monitored HupA concentrations in the ECF of the hippocampal CA1 region. The measured HupA concentrations aligned with PK behaviors observed in plasma and tissue. Additionally, neurotransmitter dynamics, particularly ACh, were tracked during drug administration.

Given the high brain retention of HupA, LC-MS/MS was employed to examine neurotransmitter changes across multiple brain regions. Both traditional tissue sampling and microdialysis revealed a significant increase in ACh levels in the hippocampal CA1 region following administration. This effect is attributed to HupA's action as a cholinesterase inhibitor, which elevates ACh concentrations and confers neuroprotective effects. Integrating these findings with prior PK data from plasma, tissue, and ECF, we developed an mPBPK-PD model to predict temporal changes in HupA and ACh in the brain. The mPBPK-PD model supports cross-species dose extrapolation from animals to humans by parameterizing physiological factors such as organ blood flow, BBB permeability, and enzyme/transporter abundance. It quantitatively predicts brain-targeted exposure and characterizes the dose-response relationship using PD markers, facilitating first-in-human dose selection and optimization of dosage regimens. Furthermore, by incorporating pathophysiological parameters, such as biomarkers of BBB disruption, into PK profiles, the model enables dose optimization under disease-altered conditions. It also allows simulation of complex dosing regimens, supporting more accurate evaluation of dosing intervals, cumulative risk, and potential drug–drug interactions in combination therapies. Model optimization and external validation enhance understanding of HupA's PK behavior and provide valuable insights for developing individualized treatment plans, optimizing dosing strategies, and assessing drug safety and efficacy.

MCAO is a stable, reproducible, and low-mortality model of cerebral ischemia. We investigated the PK behavior of HupA in the MCAO model and observed a marked increase in plasma drug exposure under pathological conditions, accompanied by variable increases in brain drug exposure. These results indicate that cerebral ischemia substantially alters HupA's PK. We further examined HupA's effects on brain neurotransmitter levels in the MCAO model and found a strong correlation between HupA concentration and ACh fluctuations in the striatal region. These findings suggest that HupA effectively elevates ACh levels and ameliorates various biochemical and metabolic abnormalities associated with cerebral ischemia, offering new directions for research into the pathophysiology, prevention, and treatment of ischemic brain injury. In the normal state, repeated dosing resulted in decreased plasma exposure but increased drug accumulation in the brain, particularly in the Hc and STR. Under ischemic conditions, both plasma and brain exposure levels rose, with the most pronounced increases observed in the parietal lobe, temporal lobe, and STR. Cerebral ischemia disrupts the structure and function of the BBB, leading to degradation of tight junction proteins (TJPs) [51–52], basement membrane damage, and pericyte dysfunction. In the MCAO model, ischemia-reperfusion injury induces oxidative stress and inflammation, promoting the release of pro-inflammatory cytokines (e.g., TNF-α, IL-1β) [53] and activation of matrix metalloproteinases (MMPs). These enzymes degrade TJPs (e.g., occludin, claudin-5) and basement membrane components (e.g., laminin), thereby increasing BBB permeability. Consequently, due to its low molecular weight and high lipophilicity, HupA crosses the BBB more readily *via* paracellular or transcellular routes [54-57]. In summary, the altered PK under cerebral ischemia suggests that while these changes may enhance therapeutic efficacy, they also elevate the risk of adverse effects. Therefore, careful dose adjustment based on patient-specific conditions is necessary to minimize potential side effects.

The PD effects of HupA are closely linked to its ability to

modulate neurotransmitter systems in the brain. As an AChE inhibitor, HupA increases ACh levels, which has been shown to improve cognitive function in both AD and VaD patients [17, 58-61]. Moreover, HupA exhibits neuroprotective effects against ischemia-induced injury, likely mediated by its cholinergic anti-inflammatory properties [62-65]. In our study, HupA administration led to significant increases in ACh levels and other neurotransmitters, including NE, DA, and GABA, indicating broad neuroprotective activity across multiple pathways. The elevation of NE and DA may result from indirect activation of the cholinergic system by HupA. Experimental evidence indicates a direct correlation between fluctuations in DA and ACh concentrations in the brain [66–67]. NE and DA, which regulate motor function, motivation, and cognition, may contribute to improvements in attention, memory consolidation, and motivational behaviors through enhanced release [68–69]. Additionally, neurotransmitter alterations observed in the MCAO model, including reductions in Glu and serotonin (5-HT), align with mechanisms underlying cognitive dysfunction in ischemic conditions [70–71]. Studies have shown that cerebral ischemia disrupts monoamine neurotransmitter balance [72], with declines in DA, NE, and 5-HT contributing to PSD. HupA administration appears to modulate these neurotransmitters, potentially mitigating such complications [73].

Conclusion

Overall, our findings demonstrate that HupA displays alteredPK and enhanced brain accumulation under ischemic conditions,resulting in significant modulation of key neurotransmitters, in-cluding ACh, DA, and NE. We developed an mPBPK-PD modelcapable of accurately predicting brain-targeted drug exposureand dose–response relationships, thereby enabling rational doseoptimization across both physiological and pathological states.These results offer mechanistic insights into HupA' sneuropro-tective actions and support its targeted application in thetreat-ment of ischemic brain injury and other CNS disorders.

Funding

This work was supported by the National Key Research and Development Program of China (No. 2024YFA1308200), the National Natural Science Foundation of China (Nos. 82274009 and 81973556).

Acknowledgments

We gratefully acknowledge the use of BioRender for the creation of the scientific illustrations in this study.

Declaration of competing interest

These authors have no conflict of interest to declare.

References

1 Le TTM, Hoang ATH, Nguyen NP, et al. A novel huperzine A-producing endophytic fungus *Fusarium* sp. Rsp5.2 isolated from *Huperzia serrate*. *Biotechnol Lett*. 2020;42(6):987-995. https://doi.org/10.1007/s10529-020-02836-x.
2 Ferreira A, Rodrigues M, Fortuna A, et al. Huperzine A from *Huperzia serrata*: a review of its sources, chemistry, pharmacology and toxicology. *Phytochem Rev*. 2016;15(1):51-85. https://doi.org/10.1007/s11101-014-9384-y.
3 Luo ZW, Yin FC, Wang XB, et al. Progress in approved drugs from natural product resources. *Chin J Nat Med*. 2024;22(3):195-211. https://doi.org/10.1016/s1875-5364(24)60582-0.
4 Zhang RW, Tang XC, Han YY, et al. Drug evaluation of huperzine A in the treatment of senile memory disorders. *Acta Pharmacol Sin*.1991;12(3):250-252.
5 Tsai SJ. Huperzine A, a versatile herb, for the treatment of Alzheimer's disease. *J Chin Med Assoc*. 2019;82(10):750-751. https://doi.org/10.1097/jcma.0000000000000151.
6 Wang LS, Zhou J, Shao XM, et al. Huperzine A attenuates cognitive deficits and brain injury in neonatal rats after hypoxia–ischemia. *Brain Res*. 2002;949(1-2):162-170. https://doi.org/10.1016/s0006-8993(02)02977-3.
7 Hu Q, Zhang R, Dong X, et al. Huperzine A ameliorates neurological deficits after spontaneous subarachnoid hemorrhage through endothelial cell pyroptosis inhibition. *Acta Biochim Biophys Sin*. 2024;56(4):645-656. https://doi.org/10.3724/abbs.2024037.
8 Zhang HY, Zheng CY, Yan H, et al. Potential therapeutic targets of huperzine A for Alzheimer's disease and vascular dementia. *Chem Biol Interact*. 2008;175(1-3):396-402. https://doi.org/10.1016/j.cbi.2008.04.049.
9 Damar U, Gersner R, Johnstone JT, et al. Huperzine A as a neuroprotective and antiepileptic drug: a review of preclinical research. *Expert Rev Neurother*. 2016;16(6):671-680. https://doi.org/10.1080/14737175.2016.1175303.
10 Du Y, Liang HY, Zhang LM, et al. Administration of Huperzine A exerts antidepressant-like activity in a rat model of post-stroke depression. *Pharmacol Biochem Behav*. 2017;158:32-38. https://doi.org/10.1016/j.pbb.2017.06.002.
11 Zhou LY, Chen D, Guo XR, et al. Intravitreal injection of Huperzine A promotes retinal ganglion cells survival and axonal regeneration after optic nerve crush. *Front Cell Neurosci*. 2023;17:1145574. https://doi.org/10.3389/fncel.2023.1145574.
12 Yang XY, Geng L, Li R, et al. Huperzine A-liposomes efficiently improve neural injury in the hippocampus of mice with chronic intermittent hypoxia. *Int J Nanomed*. 2023;18:843-859. https://doi.org/10.2147/ijn.s393346.
13 An JR, Zhao YS, Luo LF, et al. Huperzine A, reduces brain iron overload and alleviates cognitive deficit in mice exposed to chronic intermittent hypoxia. *Life Sci*. 2020;250:117573. https://doi.org/10.1016/j.lfs.2020.117573.
14 Liang YQ, Tang XC. Comparative studies of huperzine A, donepezil, and rivastigmine on brain acetylcholine, dopamine, norepinephrine, and 5-hydroxytryptamine levels in freely-moving rats. *Acta Pharmacol Sin*. 2006;27(9):1127-1136. https://doi.org/10.1111/j.1745-7254.2006.00411.x.
15 Li F, Hu RF, Wang B, et al. Self-microemulsifying drug delivery system for improving the bioavailability of huperzine A by lymphatic uptake. *Acta Pharm Sin B*. 2017;7(3):353-360. https://doi.org/10.1016/j.apsb.2017.02.002.
16 Zhang RH, Wang C, Shi T, et al. Pharmacokinetics of HupA-PLGA-NPs of different sizes in the mouse blood and brain determined by LC-MS/MS. *Eur Rev Med Pharmacol Sci*. 2022;26(4):1183-1195. https://doi.org/10.26355/eurrev_202202_28111.
17 Singh YP, Kumar H. A recent update on huprine and its hybrids as a potential multifunctional agent for the treatment of Alzheimer's disease. *Chem Biol Drug Des*. 2024;103(2):e14478. https://doi.org/10.1111/cbdd.14478.
18 Xu WJ, Zhang HY. Progress in clinical studies of huperzine a on improvement of cognitive function. *Chin J New Drugs Clin Remed*. 2012;31(12):707-712. https://doi.org/10.1007/s11783-011-0280-z. https://doi.org/10.1007/s11783-011-0280-z.
19 Guo XR, Wu YH, Wang QQ, et al. Huperzine A injection ameliorates motor and cognitive abnormalities *via* regulating multiple pathways in a murine model of Parkinson's disease. *Eur J Pharmacol*. 2023;956:175970. https://doi.org/10.1016/j.ejphar.2023.175970.
20 Judd JM, Jasbi P, Winslow W, et al. Inflammation and the pathological progression of Alzheimer's disease are associated with low circulating choline levels. *Acta Neuropathol*. 2023;146(4):565-583. https://doi.org/10.1007/s00401-023-02616-7.
21 Cao Y, Jusko WJ. Applications of minimal physiologically-based pharmacokinetic models. *J Pharmacokinet Pharmacodyn*. 2012;39(6):711-723. https://doi.org/10.1007/s10928-012-9280-2.
22 Ayyar VS, Lee JB, Wang W, et al. Minimal physiologically-based pharmacokinetic (mPBPK) metamodeling of target engagement in skin informs anti-IL17A drug development in psoriasis. *Front Pharmacol*. 2022;13:862291. https://doi.org/10.3389/fphar.2022.862291.
23 Krzyzanski W, Milad MA, Jobe AH, et al. Minimal physiologically-based hybrid model of pharmacokinetics in pregnant women: application to antenatal corticosteroids. *CPT Pharmacom Syst Pharma*. 2023;12(5):668-680. https://doi.org/10.1002/psp4.12899.
24 Ogawa Y, Tsugita S, Torii Y, et al. Microdialysis-integrated HPLC system with dual-electrode detection using track-etched membrane electrodes for *in vivo* monitoring of dopamine dynamics. *J Chromatogr B*. 2024;1247:124318. https://doi.org/10.1016/j.jchromb.2024.124318.
25 Halfhide C, Cammarano TL, Anderson KA, et al. Using microdialysis to monitor dopaminergic support of limb-use control following mesencephalic neurosphere transplantation in a rodent model of Parkinson's Disease. *Behav Brain Res*. 2024;471:115121. https://doi.org/10.1016/j.bbr.2024.115121.
26 Longa EZ, Weinstein PR, Carlson S, et al. Reversible middle cerebral artery occlusion without craniectomy in rats. *Stroke*. 1989;20(1):84-91. https://doi.org/10.1161/01.str.20.1.84.
27 Bederson JB, Pitts LH, Tsuji M, et al. Rat middle cerebral artery occlusion: evaluation of the model and development of a neurologic examination. *Stroke*. 1986;17(3):472-476. https://doi.org/10.1161/01.str.17.3.472.
28 Riglet F, Mentre F, Veyrat-Follet C, et al. Bayesian individual dynamic predictions with uncertainty of longitudinal biomarkers and risks of survival events in a joint modelling framework: a comparison between stan, monolix, and NONMEM. *AAPS J*. 2020;22(2):50. https://doi.org/10.1208/s12248-019-0388-9.
29 Sang L, Yuan Y, Zhou Y, et al. A quantitative systems pharmacology approach to predict the safe-equivalent dose of doxorubicin in patients with cardiovascular comorbidity. *CPT Pharmacom Syst Pharma*. 2021;10(12):1512-1524. https://doi.org/10.1002/psp4.12719.
30 Djerada Z, Feliu C, Cazaubon Y, et al. Population pharmacokinetic-pharmacodynamic modeling of ropivacaine in spinal anesthesia. *Clin Pharmacokinet*. 2018;57(9):1135-1147. https://doi.org/10.1007/s40262-017-0617-2.

31 Van Belle K, Sarre S, Ebinger G, et al. Brain, liver and blood distribution kinetics of carbamazepine and its metabolic interaction with clomipramine in rats: a quantitative microdialysis study. *J Pharmacol Exp Ther*. 1995;272 (3):1217-1222. https://doi.org/10.1016/s0022-3565(25)24549-9.

32 Wang H, Tang XC. Anticholinesterase effects of huperzine A, E2020, and tacrine in rats. *Acta Pharmacol Sin*. 1998;19(1):27-30.

33 Li C, Shi S. Neuroprotective effect of huperzine a on d-galactose-induced hearing dysfunction. *Ear Nose Throat J*. 2021;100(3_suppl):269S-276S. https://doi.org/10.1177/0145561319864570.

34 Mak SH, Li WM, Fu HJ, et al. Promising tacrine/huperzine A-based dimeric acetylcholinesterase inhibitors for neurodegenerative disorders: From relieving symptoms to modifying diseases through multitarget. *J Neurochem*. 2021;158(6):1381-1393. https://doi.org/10.1111/jnc.15379.

35 Dineley KT, Pandya AA, Yakel JL. Nicotinic ACh receptors as therapeutic targets in CNS disorders. *Trends Pharmacol Sci*. 2015;36(2):96-108. https://doi.org/10.1016/j.tips.2014.12.002.

36 Jing M, Li YX, Zeng JZ, et al. An optimized acetylcholine sensor for monitoring *in vivo* cholinergic activity. *Nat Methods*. 2020;17(11):1139-1146. https://doi.org/10.1038/s41592-020-0953-2.

37 Tang CY, Chen T, Kapadnis S, et al. Neuropharmacokinetics of two investigational compounds in rats: divergent temporal profiles in the brain and cerebrospinal fluid. *Biochem Pharmacol*. 2014;91(4):543-551. https://doi.org/10.1016/j.bcp.2014.07.023.

38 Si JC, Chen X, Qi KR, et al. Shengmaisan combined with Liuwei Dihuang Decoction alleviates chronic intermittent hypoxia-induced cognitive impairment by activating the EPO/EPOR/JAK2 signaling pathway. *Chin J Nat Med*. 2024;22(5):426-440. https://doi.org/10.1016/s1875-5364(24)60640-0.

39 Wang D, Yan B, Wang A, et al. Tu-Xian Decoction ameliorates diabetic cognitive impairment by inhibiting DAPK-1. *Chin J Nat Med*. 2023;21(12):950-960. https://doi.org/10.1016/s1875-5364(23)60428-5.

40 Zhou JC, Fan QL, Cai XY, et al. *Ginkgo biloba* extract protects against depression-like behavior in mice through regulating gut microbial bile acid metabolism. *Chin J Nat Med*. 2023;21(10):745-758. https://doi.org/10.1016/s1875-5364(23)60496-0.

41 Coleman BR, Ratcliffe RH, Oguntayo SA, et al. [+]-Huperzine A treatment protects against *N*-methyl-D-aspartate-induced seizure/status epilepticus in rats. *Chem Biol Interact*. 2008;175(1-3):387-395. https://doi.org/10.1016/j.cbi.2008.05.023.

42 Lu HY, Lu L, Jiang M, et al. Ultrastructural mitochondria changes in perihematomal brain and neuroprotective effects of Huperzine A after acute intracerebral hemorrhage. *Neuropsychiatr Dis Treat*. 2015:2649. https://doi.org/10.2147/ndt.s92158.

43 Lin PP, Li XN, Yuan F, et al. Evaluation of the *in vitro* and *in vivo* metabolic pathway and cytochrome P450 inhibition/induction profile of Huperzine A. *Biochem Biophys Res Commun*. 2016;480(2):248-253. https://doi.org/10.1016/j.bbrc.2016.10.039.

44 Wu SL, Gan J, Rao J, et al. Pharmacokinetics and tolerability of oral dosage forms of huperzine a in healthy Chinese male volunteers: a randomized, single dose, three-period, six-sequence crossover study. *Curr Med Sci*. 2017;37(5):795-802. https://doi.org/10.1007/s11596-017-1807-8.

45 Becchi S, Chieng B, Bradfield LA, et al. Cognitive effects of thalamostriatal degeneration are ameliorated by normalizing striatal cholinergic activity. *Sci Adv*. 2023;9(25):eade8247. https://doi.org/10.1126/sciadv.ade8247.

46 Valdés Hernández MDC, Case T, Chappell FM, et al. Association between striatal brain iron deposition, microbleeds and cognition 1 year after a minor ischaemic stroke. *Int J Mol Sci*. 2019;20(6):1293. https://doi.org/10.3390/ijms20061293.

47 Chen APF, Chen L, Shi KW, et al. Nigrostriatal dopamine modulates the striatal-amygdala pathway in auditory fear conditioning. *Nat Commun*. 2023;14:7231. https://doi.org/10.1038/s41467-023-43066-9.

48 Oddo M, Hutchinson PJ. Understanding and monitoring brain injury: the role of cerebral microdialysis. *Intensive Care Med*. 2018;44(11):1945-1948. https://doi.org/10.1007/s00134-017-5031-6.

49 Peerdeman SM, Girbes ARJ, Vandertop WP. Cerebral microdialysis as a new tool for neurometabolic monitoring. *Intensive Care Med*. 2000;26(6):662-669. https://doi.org/10.1007/s001340051230.

50 Eiden M, Christinat N, Chakrabarti A, et al. Discovery and validation of temporal patterns involved in human brain ketometabolism in cerebral microdialysis fluids of traumatic brain injury patients. *eBioMedicine*. 2019;44:607-617. https://doi.org/10.1016/j.ebiom.2019.05.054.

51 Wei CC, Kong YY, Hua X, et al. NAD replenishment with nicotinamide mononucleotide protects blood–brain barrier integrity and attenuates delayed tissue plasminogen activator-induced haemorrhagic transformation after cerebral ischaemia. *British J Pharmacol*. 2017;174(21):3823-3836. https://doi.org/10.1111/bph.13979.

52 Li WL, Shi JF, Yu ZY, et al. SLC22A17 as a cell death-linked regulator of tight junctions in cerebral ischemia. *Stroke*. 2024;55(6):1650-1659. https://doi.org/10.1161/strokeaha.124.046736.

53 Liu SM, Jia XP, Liu B, et al. Suppression of cerebral ischemia injury induced blood brain barrier breakdown by dexmedetomidine *via* promoting CCN1. *Aging*. 2024;16(4):3750-3762. https://doi.org/10.18632/aging.205557.

54 Gao HM, Chen H, Cui GY, et al. Damage mechanism and therapy progress of the blood-brain barrier after ischemic stroke. *Cell Biosci*. 2023;13(1):196. https://doi.org/10.1186/s13578-023-01126-z.

55 Wang XN, Liu YS, Sun YY, et al. Blood brain barrier breakdown was found in non-infarcted area after 2-h MCAO. *J Neurol Sci*. 2016;363:63-68. https://doi.org/10.1016/j.jns.2016.02.035.

56 Chen XY, Wan SF, Yao NN, et al. Inhibition of the immunoproteasome LMP2 ameliorates ischemia/hypoxia-induced blood–brain barrier injury through the Wnt/*β*-catenin signalling pathway. *Mil Med Res*. 2021;8(1):62. https://doi.org/10.1186/s40779-021-00356-x.

57 Lochhead JJ, Ronaldson PT, Davis TP. The role of oxidative stress in blood–brain barrier disruption during ischemic stroke: Antioxidants in clinical trials. *Biochem Pharmacol*. 2024;228:116186. https://doi.org/10.1016/j.bcp.2024.116186.

58 Wang HY, Wu M, Diao JL, et al. Huperzine A ameliorates obesity-related cognitive performance impairments involving neuronal insulin signaling pathway in mice. *Acta Pharmacol Sin*. 2020;41(2):145-153. https://doi.org/10.1038/s41401-019-0257-1.

59 Li JJ, Meng XG, Li F, et al. Huperzine A combined with hyperbaric oxygen on the effect on cognitive function and serum hypoxia-inducible factor-1α Level in elderly patients with vascular dementia. *Am J Transl Res*. 2021;13(6):6897-6904.

60 Li J, Wu HM, Zhou RL, et al. Huperzine A for Alzheimer's disease. In: *Cochrane Database Syst Rev*. 2008;(2):CD005592. https://doi.org/10.1002/14651858.CD005592.pub2.

61 Xing SH, Zhu CX, Zhang R, et al. Huperzine a in the treatment of Alzheimer's disease and vascular dementia: a meta-analysis. *Evid-Based Compl Alt*. 2014;2014:363985. https://doi.org/10.1155/2014/363985.

62 Huang WP, Zhu SZ, Liu XQ, et al. Cholinergic anti-inflammatory pathway involves in the neuroprotective effect of huperzine A on sepsis-associated encephalopathy. *Chin Crit Care Med*. 2016;28(5):450-454.

63 Wang ZF, Wang J, Zhang HY, et al. Huperzine A exhibits anti-inflammatory and neuroprotective effects in a rat model of transient focal cerebral ischemia. *J Neurochem*. 2008;106(4):1594-1603. https://doi.org/10.1111/j.1471-4159.2008.05504.x.

64 Zhang C, Li MG, Xie W, et al. Administration of Huperzine A microspheres ameliorates myocardial ischemic injury *via* α7nAChR-dependent JAK2/STAT3 signaling pathway. *Eur J Pharmacol*. 2023;940:175478. https://doi.org/10.1016/j.ejphar.2022.175478.

65 Su JQ, Chen KS, Sang X, et al. Huperzine a ameliorates sepsis-induced acute lung injury by suppressing inflammation and oxidative stress *via* α7 nicotinic acetylcholine receptor. *Int Immunopharmacol*. 2024;141:112907. https://doi.org/10.1016/j.intimp.2024.112907.

66 Liu C, Cai X, Ritzau-Jost A, et al. An action potential initiation mechanism in distal axons for the control of dopamine release. *Science*. 2022;375(6587):1378-1385. https://doi.org/10.1126/science.abn0532.

67 Krok AC, Maltese M, Mistry P, et al. Intrinsic dopamine and acetylcholine dynamics in the striatum of mice. *Nature*. 2023;621(7979):543-549. https://doi.org/10.1038/s41586-023-05995-9.

68 Delaney J, Nathani S, Tan V, et al. Enhanced cognitive flexibility and phasic striatal dopamine dynamics in a mouse model of low striatal tonic dopamine. *Neuropsychopharmacology*. 2024;49(10):1600-1608. https://doi.org/10.1038/s41386-024-01868-5.

69 Scognamiglio S, Aljohani YM, Olson TT, et al. Restoration of norepinephrine release, cognitive performance, and dendritic spines by amphetamine in aged rat brain. *Aging Cell*. 2024;23(4):e14087. https://doi.org/10.1111/acel.14087.

70 Griem-Krey N, Klein AB, Clausen BH, et al. The GHB analogue HOCPCA improves deficits in cognition and sensorimotor function after MCAO *via* CaMKIIα. *J Cereb Blood Flow Metab*. 2023;43(8):1419-1434. https://doi.org/10.1177/0271678x231167920.

71 Sood A, Mehrotra A, Dhawan DK, et al. Neuroprotective effects of *Withania somnifera* on ischemic stroke are mediated *via* anti-inflammatory response and modulation of neurotransmitter levels. *Neurochem Int*. 2024;180:105867. https://doi.org/10.1016/j.neuint.2024.105867.

72 Harik SI, Yoshida S, Busto R, et al. Monoamine neurotransmitters in diffuse reversible forebrain ischemia and early recirculation: Increased dopaminergic activity. *Neurology*. 1986;36(7):971. https://doi.org/10.1212/wnl.36.7.971.

73 Zhan QY, Kong FY. Mechanisms associated with post-stroke depression and pharmacologic therapy. *Front Neurol*. 2023;14:1274709. https://doi.org/10.3389/fneur.2023.1274709.